Transport Research Laboratory
Creating the future of transport


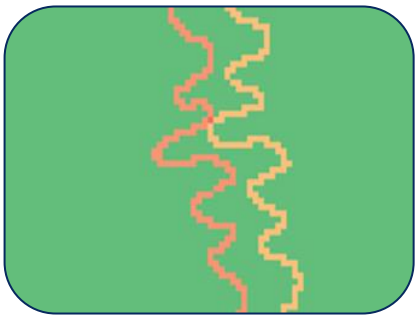
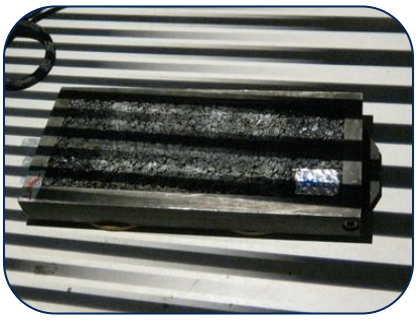

PUBLISHED PROJECT REPORT PPR740

Use of high-resolution 3-D surface data to monitor change over time on pavement surfaces

Research into pavement surface disintegration: Phase 3

Stuart McRobbie, Caroline Wallbank, Kamal Nesnas, Alex Wright

Prepared for:	Highways Agency, Network Services
Project Ref:	100(4/45/12)HALC

Quality approved:

Stuart McRobbie (Project Manager)

Alex Wright (Technical Referee)

Disclaimer

Contents amendment record

This report has been amended and issued as follows:

Version	Date	Description	Editor	Technical Referee
0.1	17/10/14	DRAFT – for TR and client comment	SMcR	AW
1.0	12/12/14	Completed DRAFT for TR comment prior to release to client	SMcR	AW
1.1	16/12/14	Redrafted following TR comments. Cosmetic and structural changes made, and comments put in to give details of outstanding changes or data required.	SMcR	AW
1.2	14/01/2015	Final draft for TR approval prior to publication. Addressed comments and made required changes.	SMcR	AW
2.0	24/03/15	Final draft following comments from TR. Ready for release.	SMcR	AW

Contents

Executive Summary

Surface disintegration is a term used to cover a range of progressive defects such as fretting or ravelling which are caused by aging of binder and loss of adhesion to aggregate. If allowed to progress unchecked surface disintegration can lead to the removal of the wearing course of a pavement, uneven surfaces and potholes. The timescale from the initiation of these defects to the point at which expensive and disruptive maintenance is required can be short, particularly on thin surfacings, which are becoming more prevalent on the Highways Agency network. A fretting algorithm has been developed by TRL and incorporated into TRACS which characterises the texture of the surface of a pavement and compares it with the surrounding pavement in order to identify areas which may be deteriorating. This approach works quite well where the fretting is quite well established and distinct from its surroundings, but by the time the TRACS algorithm detects the fretting there may be a very short window for action before the surface disintegration develops into a serious defect such as a pothole. A method which afforded the engineers responsible for maintaining the network more warning of potential deterioration would therefore be desirable.

The research presented herein follows two main strands and builds on work previously undertaken by TRL for the Highways Agency. The two strands of work are 1) the development of improved and accurate methods for aligning data from successive surveys, and 2) laboratory testing and investigation into the use of high-resolution 3-D parameters for identifying the onset of surface disintegration at a stage prior to that which can be detected by the existing TRACS fretting algorithms.

Previous research has indicated that development of an absolute measurement of surface disintegration may be very difficult, and would require detailed knowledge of the surface material. Therefore this work has investigated the development of methods for detecting and reporting changes in surface conditions, which may be indicative of surface disintegration. In order to determine whether or not a pavement is changing at a level of detail which would enable the loss of individual chips of aggregate to be detected it is vital that the data from successive surveys can be accurately and reliably aligned such that any changes in the calculated parameters are the result of genuine condition changes and not merely a side-effect of having misaligned the datasets. The work presented in this report describes the alignment methods developed. These use GPS data to perform an initial location of the data, then make use of the longitudinal profiles measured to determine how the surveys should be adjusted longitudinally. This is then followed by use of transverse profiles from successive surveys to refine the alignment and remove the effects of driving line etc. The report describes the development of the methods, and the experimental work performed to validate it against reference data.

The development of the change parameter has been investigated using high-resolution 3-D surface measurements made on a set of lab samples with a high-resolution Breuckmann SmartSCAN stereo imaging system. This work has involved the collection of surface measurements during a process of accelerated wear on the samples which was designed to mimic the types of change which occur on network sites. By processing and analysing the measurements it has been possible to develop a change parameter which has been seen to produce different results on trafficked parts of the sample to those produced where little or no trafficking was taking place.

1 Introduction

The loss of surface chippings or aggregate from the surface of a pavement (ravelling, fretting, or surface disintegration) is a major problem for those responsible for maintaining the condition of the road (Scott, Radband, Zohrabi, Sanders, McRobbie, & Wright, 2008). Factors such as age, traffic and weather cause the binder to harden, allowing the aggregate to be removed (Figure 1), which leads to costly and disruptive maintenance. If allowed to progress unchecked the defect can result in the complete removal of the wearing course of a pavement, leading to potholes.

Figure 1: Example of ravelling on Hot Rolled Asphalt.

This loss of surface material can occur at any time. However, on a well-constructed pavement, the defect is more likely to occur later in the pavement's life as a result of fatigue or weathering. The defect primarily affects the pavement longevity, typically by permitting water to get in, but can also affect the safety, comfort and noise perception of road users. It is therefore a defect of concern to the road owner.

Most of the UK primary road network is surfaced with either Hot Rolled Asphalt (HRA), or thin surfacing materials. The different construction methods of these surfaces mean that they deteriorate in different ways. This is particularly true for the way in which they lose aggregate as they age. The aggregate in an HRA pavement is rolled and pressed into the binder which is already spread on the surface of the pavement. The aggregate in a thin surfacing material is typically much smaller than that used on an HRA pavement, and is mixed in with the binder before being applied to the pavement.

Loss of surface material from HRA surfaces starts to occur as the binder hardens and loses its adhesion. This results in individual chippings being removed from the surface which can give the pavement a pock-marked appearance. As the defect progresses the number of missing chips will increase until the holes left behind by the removed aggregate can join up and begin to form potholes over a long period of time.

On thin surfaces and porous asphalt the surface disintegration begins with localized loss of aggregate, which accelerates as adjacent aggregate is dislodged from the surface as a result of trafficking. However, because of the smaller aggregate and the different construction method the appearance is different to that on HRA, with the loss of any individual chip being less obvious visually. This deterioration is often referred to as ravelling, and can result in the total loss of the surface layer. The time from the initiation of the defect (or at least the point at which the defect becomes noticeable during a routine visual survey) and the total removal of the surface material can be relatively short (in comparison with the speed of defect progression on HRA). This makes it hard for the engineer to efficiently plan the maintenance of the pavement, and increases the

importance of trying to provide as much advance warning of the defect being present as possible.

The pictures shown in Figure 2 to Figure 5 illustrate the appearance of ravelling at 4 different levels. These levels can be loosely defined as:

- Level 0 – No visible signs of ravelling (Figure 2);
- Level 1 – Possible signs of ravelling (Figure 3);
- Level 2 – Definite signs of ravelling (Figure 4);
- Level 3 – Serious ravelling (Figure 5).

Figure 2: Level 0 – No visible signs of ravelling

Figure 3: Level 1 – Possible signs of ravelling

Figure 4: Level 2 – Definite signs of ravelling

Figure 5: Level 3 – Serious ravelling

Specifying when a surface stops being "Level 0", and begins to be "Level 1" (and similarly for levels 1-2, and 2-3) is not easy to define and results in subjective, variable and hard to reproduce condition reports.

To obtain best value in the operation and maintenance of a road network it is imperative that road renewal schemes are accurately prioritised to ensure that the most beneficial schemes go ahead at the right time. For this reason a reliable way of detecting ravelling at an early stage in the development of the defect is highly desirable.

The research described in this report is the third stage in an ongoing process to provide a better understanding of what the early signs of aggregate loss are, and if possible, develop appropriate measurement tools and techniques to provide engineers with an increased period between the detection of the defect, and the time at which it has progressed to require more disruptive and costly maintenance action.

2 Review of other work on detection of surface disintegration

Research into automated methods of detecting surface disintegration and associated defects has been going on for more than a decade now. Early developments were carried out in the Netherlands where van Ooijen et al. (2004) developed algorithms which were capable of detecting loss of aggregate in porous asphalt, using data from a single texture laser.

The ideas in this early work were developed by TRL on behalf of the HA, to be applicable first of all on HRA in the wheelpath (Wright, 2004), then to use data from across the whole carriageway (Mays, Wright, & Furness, 2006), and to work across the carriageway regardless of surface material ((Furness & Wright, 2007), (McRobbie, Iaquinta, & Wright, 2009)).

A review of other work relevant to the detection of surface disintegration was undertaken to ensure that all recent developments were considered in the development.

2.1 Highways Agency Surface Disintegration research

Phase 1 of the research (McRobbie, Iaquinta, & Wright, 2011) considered the use of the network level measure developed for use with TRACS data. This uses data collected by 7 profile measurement lasers to characterise the pseudo-texture of the pavement over short, local lengths, and longer, global lengths. If the local texture is significantly different to the global texture, and certain other criteria are met, then the local length is deemed to be fretted and this is reported in the TRACS outputs. This approach relies on a number of assumptions: most of the surface of the Highways Agency network will not be fretted; where fretting is present it will be in relatively short lengths; where fretting is present the local texture will be higher than the global texture due to the removal of aggregate.

It was concluded that the parameters delivered by this method are helpful in identifying which parts of a given network exhibit more or less surface disintegration, but the methodology detects areas where the defect is already quite well established. Hence the methodology would not be suitable for detecting the early signs of fretting, when the condition of a pavement is moving from Level 0 to Level 1 (see Figure 2 and Figure 3). Consequently, alternative measurement techniques and methods of detecting the early stages of deterioration and aggregate loss were considered. It was concluded that the early development of surface disintegration might be detected by measuring the surface shape of the pavement at a high level of detail and developing a tool capable of detecting changes in this highly detailed data from survey to survey. Therefore a review of available measurement technologies was carried out, which concluded that in order to detect the small physical changes which were of interest a very high-resolution 3-D measurement system would be required. A Breuckmann smartSCAN HE therefore was procured on behalf of the Highways Agency, as shown in Figure 6, and Figure 7.

Figure 6: Breuckmann SmartSCAN HE system showing its two cameras on either side of the central lighting unit.

Figure 7: Breuckmann SmartSCAN HE system mounted on tripod with the lighting unit projecting one of a series of patterns used in the calculation of 3-D profile.

The initial work with the Breuckmann system found that it was possible to measure accurate 3-D representations of surfaces, and that it was possible to visually detect changes in the condition of these surfaces (Figure 8), suggesting that such data could be used to detect change and hence potentially identify the onset and progression of surface disintegration.

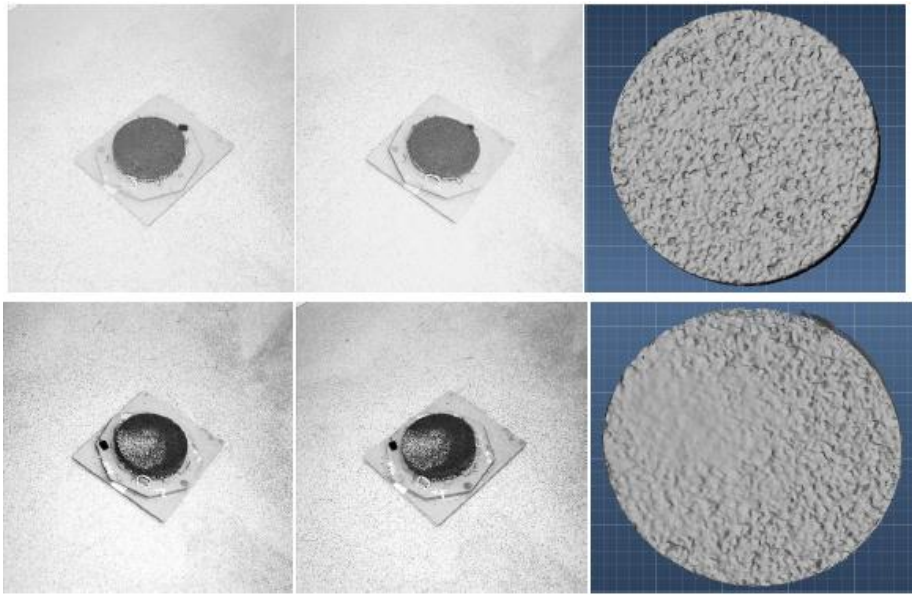

Figure 8: Images and 3-D models of cores without (top) and with (bottom) addition of sand to alter texture depth.

Phase 2 of the research (McRobbie S. , Iaquinta, Kennedy, & Wright, 2013) involved the development of a mobile platform to enable the Breuckmann system to be used on real sites and not restricted to laboratory testing. The research also involved the extraction and analysis of a range of 3-D profile and volumetric parameters from the data recorded by the Breuckmann. Parameters were calculated on 3-D profile data collected before and after forced changes in shape. Principal Component Analysis (PCA) techniques were used to reduce the number of parameters presented to end users down to three key parameters that highlighted locations that had changed. The work in Phase 2 concluded that a better understanding of how surface disintegration begins, and what physical changes can be measured in the early stages was required. The recommendation was that further work should be undertaken, either on real sites, or in the laboratory, where sites or samples could be monitored over time, and regular high-resolution 3-D measurements made as the surface condition deteriorates. The extracted volumetric parameters could then be analysed and studied to identify which parameters reflected the early signs of the genuine changes which take place during the progression of the defect under realistic conditions of trafficking and wear, as opposed to the more artificial surface condition changes which were induced in Phase 2. This would help to establish the key parameters of interest, and the data resolution and density required for the collection of shape data for future TRACS specifications and contracts.

The Phase 2 report also concluded that any practical surface disintegration measure would be likely to employ a measurement of change in condition over time, and not employ an absolute indicator of condition at a single point in time. For this to succeed it would be necessary to accurately and reliably align data from successive surveys to guarantee that any detected changes were genuine, and not merely a result of comparing different parts of the pavement from year to year. In order to facilitate this

alignment it was therefore also recommended that research be carried out into improved methods of aligning data.

The research in this, Phase 3 of the programme, has followed on from the recommendations made in Phase 2, and is attempting to improve the understanding of what occurs as surface disintegration is initiated and progresses. The aims of the work are to:

- Understand which parameters can be used to indicate possible early signs of disintegration and how these can be measured and quantified.
- Understand how these parameters change over time and how the changes relate to changes in surface disintegration.
- Develop methods for accurately and reliably aligning 3-D profile data from successive surveys.
- Propose the minimum requirements for measurements and data to enable early detection of surface disintegration in TRACS.

2.2 Literature review

The use of photogrammetry as a measurement technique for monitoring pavement surface condition and detecting surface defects has been investigated previously (Ahmed & Haas, 2010). The focus of this work has, thus far, been on crack detection with little or no attempt having been made to investigate how the data could be used to monitor surface disintegration.

Data extracted from images of pavement surfaces has been used by Elunai et al., (2010) to model the macrotexture of the imaged surface and to try to relate these extracted parameters to the measured SMTD. This research has looked at the use of Fast Fourier Transforms (FFT), autocorrelation of images, and wavelets. The research demonstrated good levels of correlation between the measured SMTD and the parameters extracted from the images using all three methods (wavelets, autocorrelation, FFT), but has not attempted to use the parameters to monitor, detect or characterise deterioration. Work conducted on behalf of the Highways Agency has also looked at using data from images as a method of detecting surface disintegration (McRobbie, Wright, Iaquinta, Scott, Christie, & James, 2010). This looked at the use of image entropy and edge density. This work found that, while it was possible to detect changes or identify deteriorated areas in individual images, the performance over large networks was not consistent.

Interest in the Netherlands in surface disintegration and ravelling on porous asphalt (PA) has continued since the early work by van Ooijen et al, with work looking at the specific issues involved in the ravelling of PA in cold weather (Huurman, Mo, & Woldekidan, 2010). This is an issue of particular concern in the Netherlands where 90% of the main road network is PA. The research considered a range of factors including tyre-aggregate interactions, pavement deformations, and temperature induced stresses in areas of binding. Although the research has led to improved understanding of the precise physical causes and factors leading to ravelling in PA, and produced recommendations of steps to overcome these in design and construction, it has not considered methods of routine monitoring, or established what parameters could be measured and monitored to look for early signs of surface disintegration.

The Laser Crack Measurement System (LCMS) has been used by a number of researchers to collect data at traffic speed which can be used in the detection of defects. The LCMS uses projected laser lines and high speed cameras to capture images and calculate pavement shape. This shape data is available every 5mm along the road in the direction of travel, at 1mm transverse resolution, covering a width of 4m. Data from this has been used to automate the characterisation of macro-texture and detect distress (Wang, Gong, Tracy, & Nguyen, 2011). It has been shown that 3-D data provides more information than 2-D data, which the LCMS can provide at 1mm spacings. The work by Wang et al. does not however present any ideas or developments in terms of how to use the data to detect defects. Other researchers have used data from the LCMS and developed a Ravelling Index (RI) to indicate the levels of deterioration on a stretch of pavement (Laurent, Hebert, Lefebvre, & Savard, 2012). The RI is a measurement of the volume of aggregate loss per unit area, i.e. how many holes are there in the pavement surface due to removed chips. The measure has been tested in the Netherlands on PA surfaces, but gives no indication of how it could be used on other surfaces without specifically tuning the parameters and thresholds. Additionally, the measure is designed to detect established ravelling, not the very early stages of the defect which are of interest in this research.

Research in Italy (Bitelli, Simone, Girardi, & Lantieri, 2012) has found that pavement texture characteristics can be accurately and reliably detected, and that 3-D data can represent the condition of the pavement as it deteriorates. This research included an evaluation of various 2-D, 3-D profile and volumetric parameters used in characterising surfaces. The investigation involved collecting data on a series of laboratory core samples, and also on real pavements, and concluded that profile, surface and volumetric parameters were potentially useful in the characterisation of pavement condition. Other work (Wang, Yan, Huang, Chu, & Abdel-Aty, 2011) has also looked at similar profile and surface parameters, as well as the use of more well established pavement texture parameters such as SMTD and MPD.

Recent work in the UK (Mathavan, Rahman, Stonecliffe-Jones, & Kamal, 2014) has investigated the use of image and profile data to detect surface disintegration. The work splits the data into a series of 250 x 250mm cells and calculates the standard deviation of the measured profile values within each cell. Each cell is then categorised as being good, average or bad based on the value of the standard deviation and a set of defined thresholds. This approach is similar to that used in the Highways Agency TRACS algorithm. Both characterise the pavement surface texture in small areas – in this case using the standard deviation of the profile measurements in a cell; in the case of TRACS, the RMS of all the individual texture profile measurements made within a small area on the pavement surface. However, the characterisation of each cell does not consider the surface material and does not consider the expected values, or surroundings. The standard deviation of profile measurements on thin surfacing will not be the same as on HRA, or High Friction Surfacing (HFS), or on PA, yet the approach proposed uses a single set of thresholds to determine cell condition.

2.2.1 Summary of literature

Although work is being undertaken into the characterisation of macrotexture surfaces using 3-D measurements, and the development of appropriate parameters, little is being done specifically looking at surface disintegration, particularly in its early stages. Some of the work being done appears to be following similar approaches to those used in

TRACS, of characterising the macro texture in small parts of the pavement and determining whether each part is good, bad or average. However most efforts appear to be considering methods only suitable for a single surface material at any time.

2.3 Consultation with experts

Prior to finalising the experimental plans for this research phase a number of pavement experts were consulted regarding current practice and knowledge in terms of identifying surface disintegration, and what signs were looked for that the defect may be progressing. The consultation also involved discussions about how the defect may be forcibly and realistically induced in laboratory samples and proposals for the subsequent practical testing.

The consultations determined that the causes of adhesion loss, binder failure and aggregate loss are well understood (UV light, freeze-thaw cycles, physical stresses, contaminants …). However little work has been completed to track changes in the surface shape as these processes take place. Consequently the changes in shape and profile indicative of imminent or incipient fretting are not distinguished from other changes in shape which take place as a pavement ages, but does not exhibit surface disintegration.

Currently engineers undertaking visual surveys look for signs that a pavement is aging and becoming prone to aggregate loss. However the signs they look for (missing chippings) are not detectable until the defect is already well on the way to becoming a problem. Engineers would greatly appreciate and value a method of detecting such changes in binder adhesion before they get so bad that aggregate loss is well established.

Discussions were also held with experts in traffic-speed data collection and processing to establish what the issues would be if any indicator developed for surface disintegration was to be integrated into future TRACS specifications, and what the limitations would be in terms of data collection and processing, as well as how the data might be used in the maintenance and asset management process. These established that for any future methodology for the detection of surface disintegration to be integrated into traffic-speed condition surveys they would have to be compatible with existing approaches. This meant that the specific methodology employed by the Breuckmann SmartSCAN to measure the 3-D surface shape would not be suitable. However, if the data and parameters produced by the Breuckmann could be collected by alternative systems then it would be possible to integrate the processing, analysis and use of the surface disintegration data with the processing and databases used.

3 Automating data alignment in 2 dimensions

3.1 Methodology and experimental design

In order to develop a change based parameter, which will look for changes in the 3-D measured profile of a surface at the level of individual stones, it is necessary to develop methods to align successive surveys at a level of accuracy which will make it possible to detect change. If the alignment is not adequate then it is impossible to state that any change in measured parameter values are down to actual condition changes, and not just due to the inclusion and exclusion of slightly different parts of the pavement in the surfaces being compared.

Traffic speed condition surveys are performed using vehicles equipped with a range of measurement and image collection systems. These vehicles produce high-resolution data regarding road shape and visual condition, accurately geo-located thanks to GPS and inertial position measurement systems. Typical output parameters from such systems include pavement rutting, longitudinal profile, cracking, fretting, crossfall, curvature, gradient, and surface texture. HARRIS2, the survey vehicle developed and operated by TRL on behalf of the Highways Agency is equipped with a downward facing imaging system capable of collecting pavement images at 1mm resolution, covering the full 4m width of a road lane. HARRIS2 also uses a scanning laser to measure the shape of the pavement surface. This system (called the PPS) is capable of recording 1000 points across the 4m width of the survey lane, every 25mm at traffic speed. Data produced using HARRIS2 is locationally aligned using GPS and inertial systems to within 2m for all surveys, and often to within 1m when conditions are favourable.

Despite improvements in location referencing systems, data from successive surveys is not perfectly aligned. Reasons for this include driving line variations, and also slight inaccuracies in location referencing systems. Routine survey data often has to be stretched or compressed in order to fit the network definitions.

To improve the quality of data alignment TRL has previously developed methods which combine GPS and inertial position information with the measured Longitudinal Profile delivered by the survey systems to optimise the longitudinal alignment between successive surveys. These developments were undertaken as part of TRL's self-funded ongoing research into improvements into all aspects of transport related research.

However the methods developed previously only align the data in the direction of travel. The research into alignment improvements carried out in this work looked to adapt the methods to also make transverse alignments, and determine the overall levels of accuracy achievable with the method.

It was proposed that the approach would work by setting one survey run to be the ‘base’ survey, and for all other surveys calculate the longitudinal and transverse alignment correction factors (every 100mm of distance travelled) which define how much the test data must be adjusted by in order to align correctly with the ‘base’ data. The calculated test shifts would then be compared against reference shift values which would be produced using visual analysis of images.

In order to develop and demonstrate this approach an experiment was performed in which multiple surveys were undertaken on a known site, on which alignment correction factors could be calculated and compared against reference correction factors, determined by manual analysis.

A site was identified on the TRL test track, shown in Figure 9.

Figure 9: Site chosen for alignment data collection on TRL test track.

This site was marked with a chalk line which was drawn to be irregularly shaped. Multiple surveys with HARRIS2 were performed on the site, collecting longitudinal and transverse profile data using the PPS, as well as downward facing images of the pavement surface. Figure 10 shows an image of the site with the chalk line marked on the pavement.

Figure 10: Image of alignment site with chalk line and markings.

3.1.1 Data collected

12 runs were performed using HARRIS2. Of these, run 3 was designated (arbitrarily) as the base run, and all other runs were aligned with respect to this one.

3.1.2 Reference data

A visual assessment of the images was carried out to create the reference data for each survey run using ChartCrack software (Figure 11). ChartCrack is software produced by TRL for processing and displaying survey data. The software can load data from a variety of different survey systems in many formats, and can calculate condition parameters based on the loaded data. The software can also load and display downward and forward facing images collected during traffic-speed condition surveys. These images can be inspected and the presence and type of any defects contained within the image can be marked and recorded. This is done by selecting the appropriate defect type from a menu, and clicking on the image wherever this defect is seen. The software can use these inputs to produce defect maps for the data, showing the location and type of all defects recorded. The resolution of the recorded defect maps can be controlled by changing the size of the grid size used in the inspection.

To produce the reference data for this work, the downward facing images from the various survey runs were loaded into ChartCrack, one at a time, and the position of the chalk line marked on the pavement was marked by clicking on the image where the line was located. The data was recorded using a grid size of 20mm square.

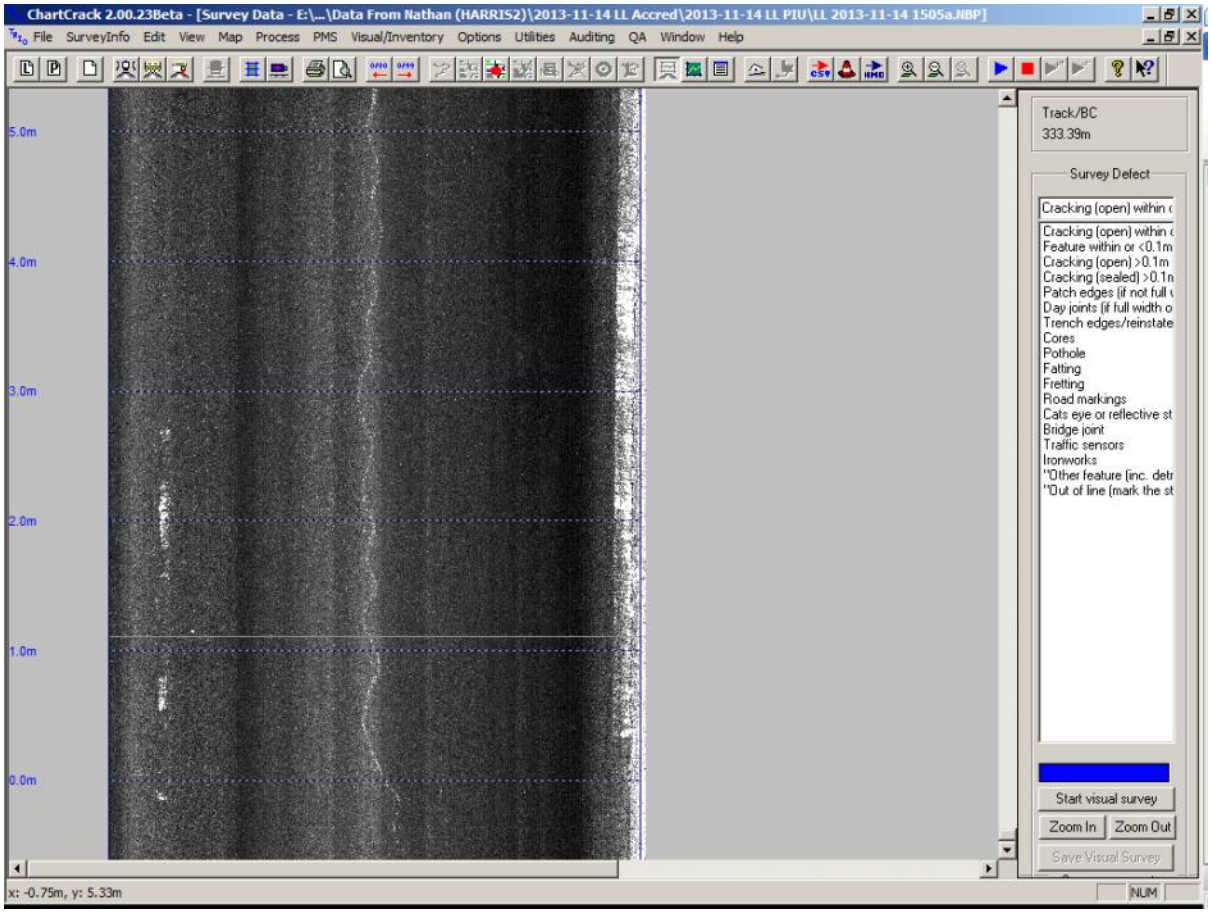

Figure 11: Screenshot of ChartCrack showing downward facing HARRIS2 images in which marked chalk line is visible.

This process generated a set of grid files in which the marked or not-marked status of each cell in the image was represented by either a 1 or a 0 (Figure 12). The positions of specific features every 100mm along the site were also noted in all datasets, and the required dx and dy correction factors (how much the data had to be moved by in the transverse and longitudinal directions) required to make the test data properly align with the base data run were calculated (Figure 13). These shifts, produced by visual inspection of the images, were used as reference data, against which the calculated shifts produced using the algorithm were compared and assessed.

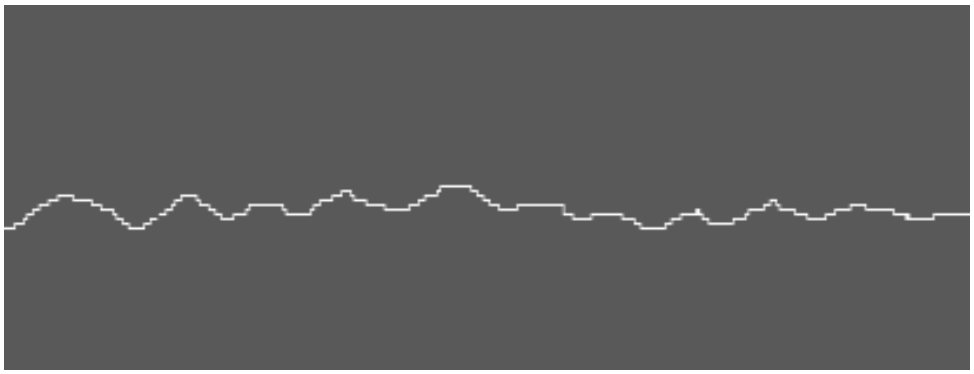

Figure 12: Output grid file, colour coded to show marked position of chalk line as white on grey background.

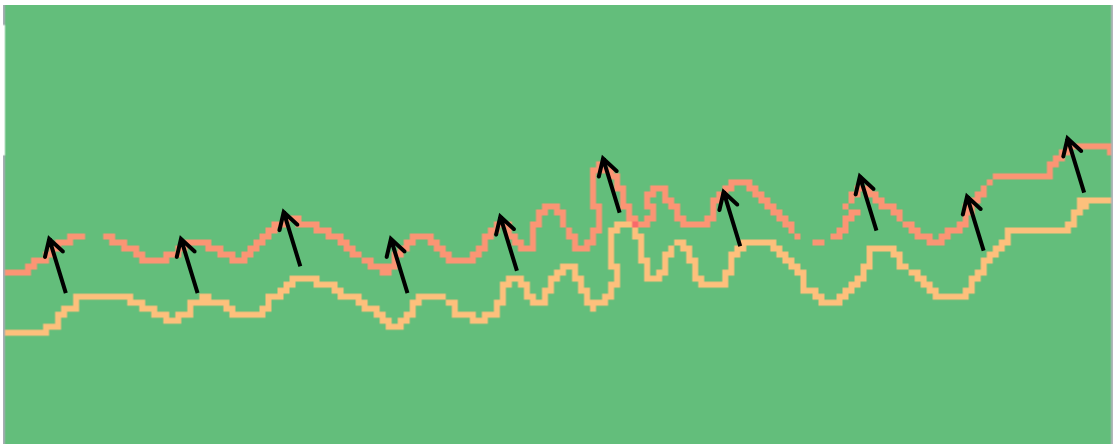

Figure 13: Display of marked line position from base data (pink) and test data (orange) used in showing reference dx and dy shifts.

The methodology developed makes a few assumptions about the data and realistic deviations that might affect it. Firstly, the data is not rotated in relation to the direction of travel. This is based on the assumption that while the driving line of the survey vehicle may vary slightly from survey to survey, it is unlikely to have severe deviations resulting in the vehicle heading in a significantly different direction in successive surveys. Additionally, it is assumed that the magnitude of transverse variation in the driving line will not be large between successive measurement points, i.e. the vehicle will not be driven such that its position on the road changes wildly from NS to OS and back again in short distances. It is also assumed that the motion of the vehicle during a survey will be in a continual forward direction, and that it will not reverse over previously surveyed parts of the road.

3.2 Development of data alignment algorithm

The longitudinal misalignment of raw condition data collected in successive surveys of the same section can be attributed to two sources of error:

1. Differences in the identification of the section change points at nodal points between surveys.

2. Differences in the measurement of distance along the length of the section.

Figure 14 shows an example of data as collected using the Pavement Profiling System (PPS) mounted on HARRIS2. The data shown in the top left is the raw measured 3-D profile, including data dropouts where no valid measurement was possible. The data shown in the top right of Figure 14 shows the profile following the removal of these dropouts, and the data shown at the bottom of Figure 14 is the resulting surface once anomalously high profile values (spikes) are removed from the data. This is the data used in the alignment process.

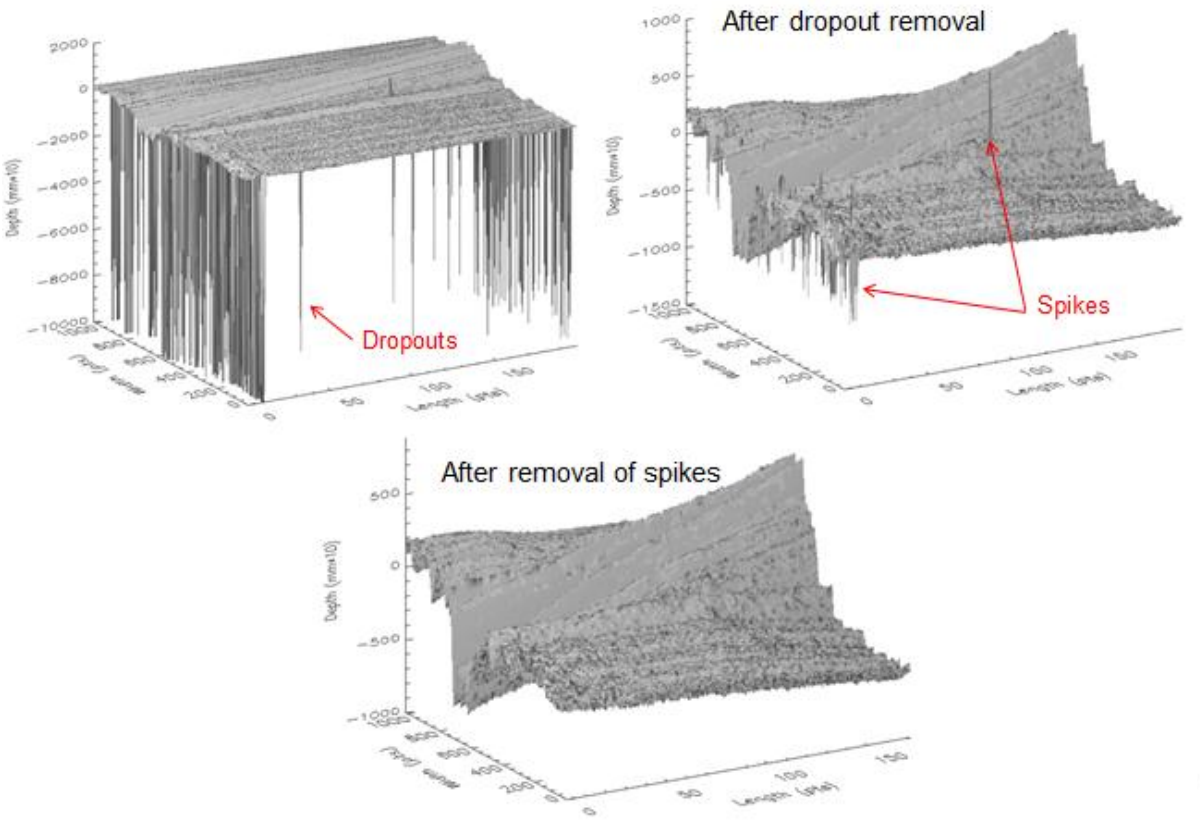

Figure 14: Example of 3-D profile measured data, before and after the removal of spikes and dropouts

The alignment of the profile data is performed in two stages: first in the longitudinal direction (i.e. the direction of travel), followed by a transverse alignment in the direction perpendicular to the direction of travel. This process of aligning the cleaned data is illustrated in Figure 15. This will be discussed in detail in the rest of section 3.2.

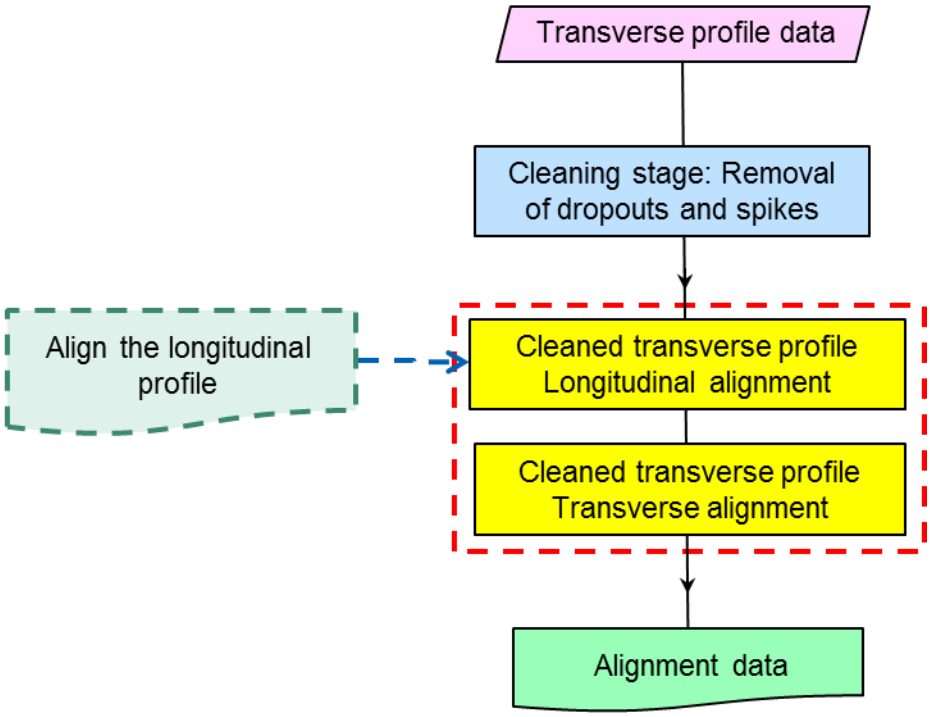

Figure 15: The stages of the alignment process

3.2.1 Longitudinal alignment

In previous research for the Highways Agency and the TSB (Technology Strategy Board) an alignment algorithm was developed to perform automatic alignment of the longitudinal profile data. This longitudinal alignment is performed in two steps: the first step aligns the profile using the GPS measurements and the (Ordnance Survey Grid Reference) OSGR data reported in each survey; the second step refines the alignment based upon similarities in the shape of the longitudinal profiles.

The process of aligning the OSGR co-ordinates consists of loading the two sets of survey data, including the longitudinal profiles, section lengths and the OSGR data. The offsets between corresponding section identifiers are obtained from the OSGR data by calculating the difference between the positions reported for the section start points in each survey as illustrated in Figure 16. The calculated offsets are then used to shift the data from one survey to achieve alignment with respect to the second survey.

Following the alignment of the data using OSGR, the alignment is refined within each section. This is done by dividing the sections into 50m subsections and calculating the correlation between the two survey profiles at a series of longitudinal offsets of one profile with respect to the other.

Figure 17 shows the calculated longitudinal offset plotted against chainage calculated for four runs against a common baseline survey. The offset values for each of the tests do not vary a great deal from the determined initial offset of the run from the baseline.

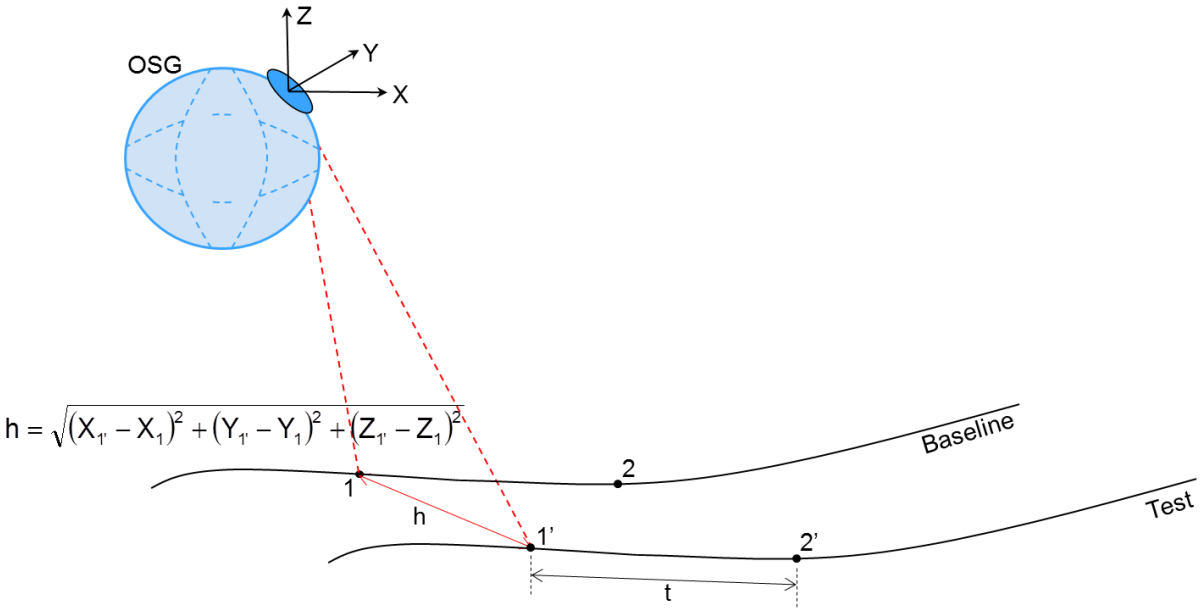

Figure 16: Use of Ordnance Survey Grid Reference Co-ordinates (OSGR) to calculate offset, h, between two surveys.

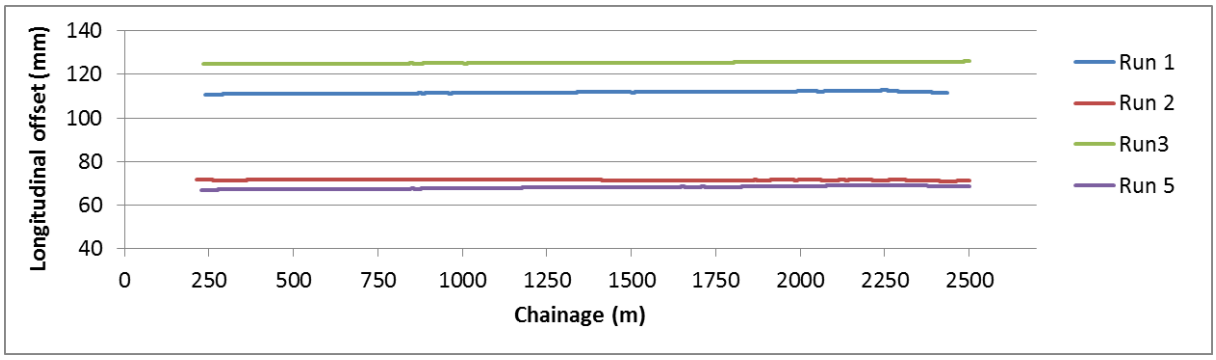

Figure 17: Longitudinal offsets required to align the baseline against the test runs

The results of applying the calculated offsets to the test profile measured during test run 1 are plotted in Figure 18, showing examples for before, and after, alignment of the data.

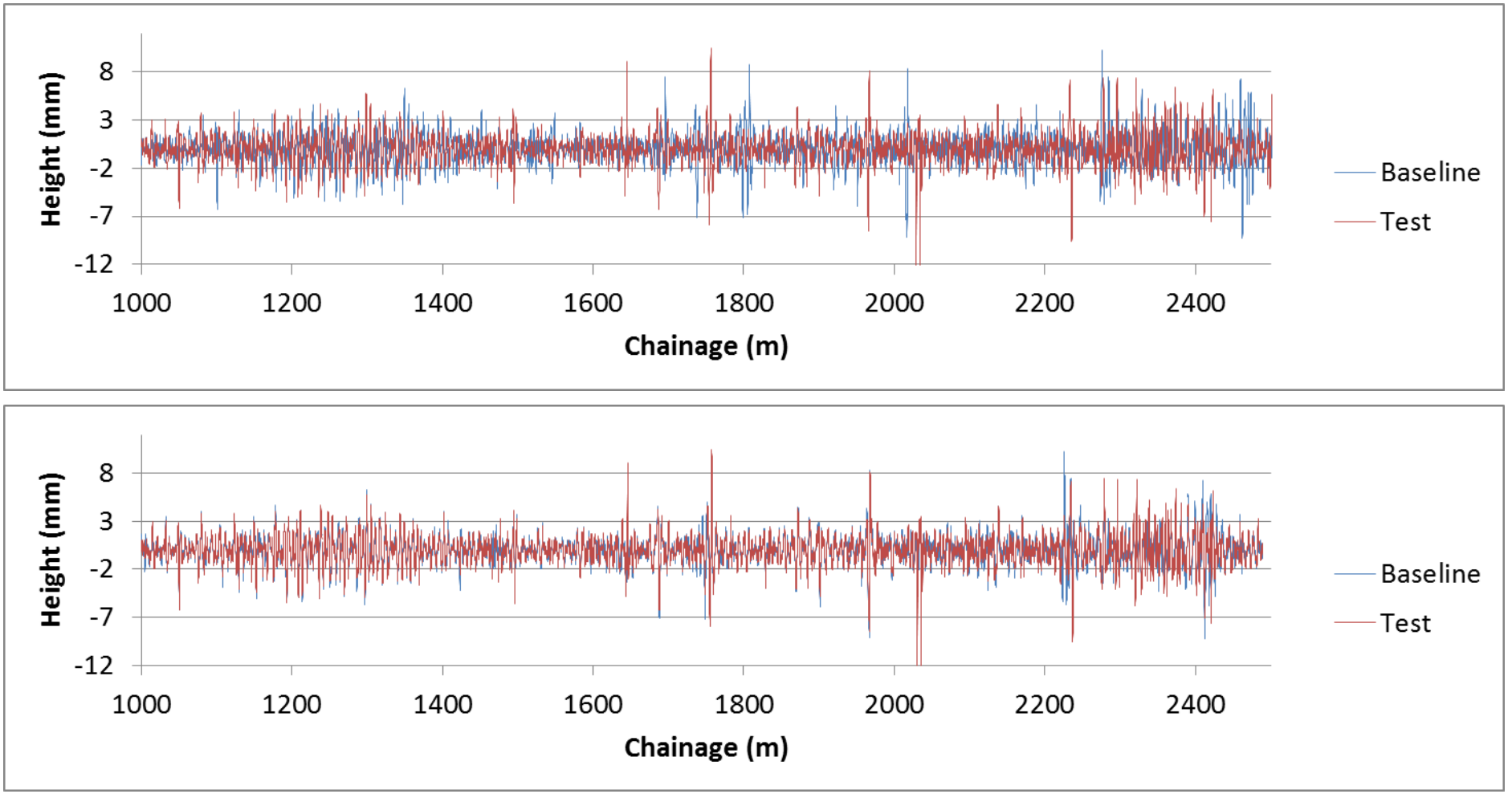

Figure 18: Example of Longitudinal profile alignment (before alignment, top; after alignment, bottom)

The improvements in the alignments of the baseline and test profiles following application of the longitudinal shifts are evident in the plots shown in Figure 18. It is however, also clear that there are still some discrepancies between the measured profiles even after longitudinal alignment (e.g. at approximately 2240m in Figure 18). These may be due to pavement features producing variations in the longitudinal profile which are localised across the pavement, and which therefore only get measured if certain driving lines are followed. Improving the transverse alignment of the data may reduce or remove these discrepancies.

The histograms of the height differences between the baseline and the test are plotted for the data before and after longitudinal alignment in Figure 19. A noticeable narrowing of the width of the distribution of the aligned data is observed. The mean and variance (μ, σ^2) of the distributions are shown in Table 1.

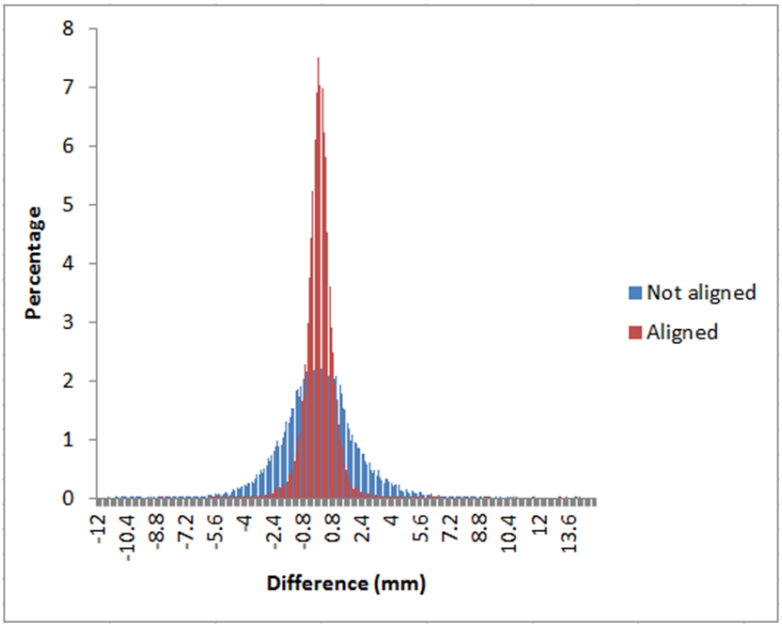

Figure 19: Histogram comparison between the baseline and the test before and after the automatic alignment.

Table 1: Mean and variance of distributions of profile height difference between test and baseline profiles before and after longitudinal alignment.

	Mean (μ)	Variance (σ^2)
Before alignment	0.001	4.411
After alignment	0.001	0.729

Following the longitudinal alignment, the data is then adjusted transversely, to improve alignment across the carriageway and remove variations which may have been introduced by changes in the driving line of the survey vehicle.

3.2.2 Transverse alignment

The stages of the transverse alignment are summarised in Figure 20: the process begins by identifying the baseline Transverse Profile (TP) which is longitudinally aligned with the test TP (using the longitudinal alignment information), the baseline and test TPs are normalised to remove road geometry, but leave pavement shape. The test TP is then

repeatedly shifted transversally with respect to the baseline TP, and the correlation between the profiles at each shift is found. The transverse shift value corresponding to the maximum correlation is determined.

However, it was found that this process does not always generate the best transverse alignment and we observed spurious maxima in the correlations and alignment factors which made no logical sense. Therefore a series of logical decision rules were developed for the calculated shift values. This is followed by testing the extremes of the shift values based on neighbourhood values around the shift values being investigated.

The process is described in further detail in the following sections.

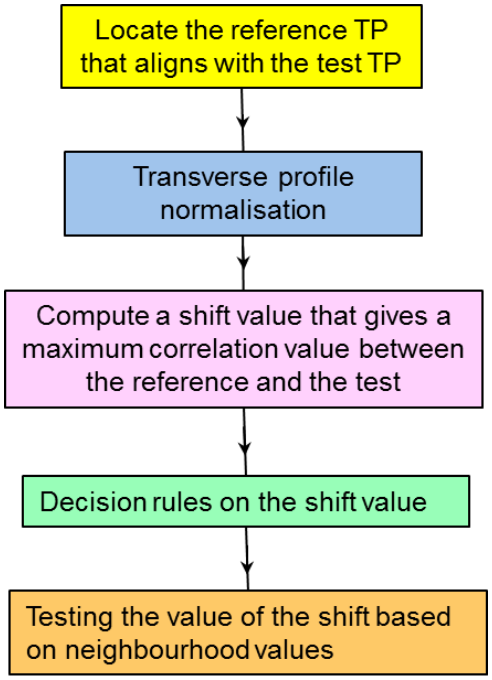

Figure 20: Flowchart describing the stages of the transverse alignment

3.2.2.1 Data Normalisation

Data normalisation is the process of removing long wavelengths from the baseline and the test TP, and also filtering to remove wavelengths less than 300mm. This removes the effect of road geometry, and also the pavement macrotexture. Including the macrotexture can result in spurious correlation maxima. Figure 21 shows two examples of baseline TP plotted against the test TP. The underlying shape of the transverse profile measured by the PPS system can be seen.

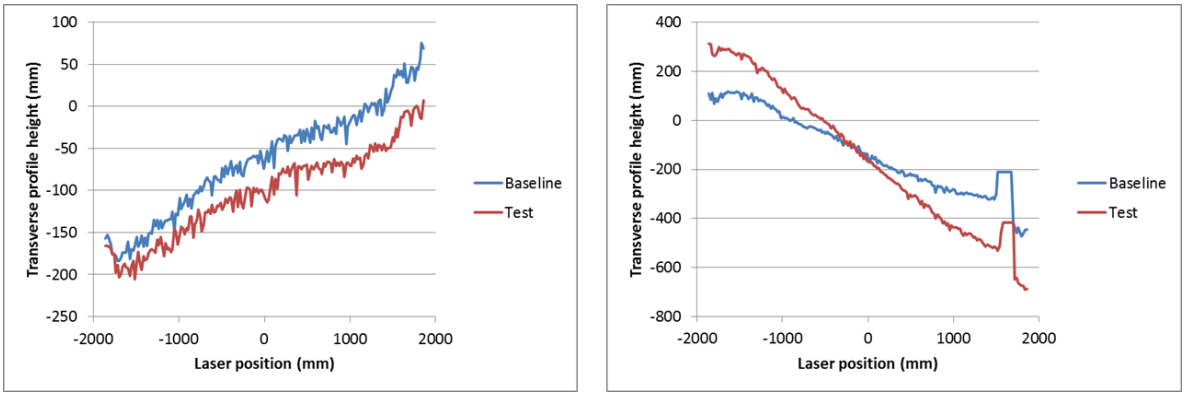

Figure 21: Two examples of aligned transverse profiles as measured by the PPS system

Figure 22 shows the same data as in Figure 21, after the normalisation process which removes long (left) and short (right) wavelengths. It can be seen in this that the normalised baseline and test profiles are similar, with slight offsets. For example the test profile (red) in the left hand plot in Figure 22 must be shifted slightly to the left by approx. 200mm in order to be optimally aligned with the baseline.

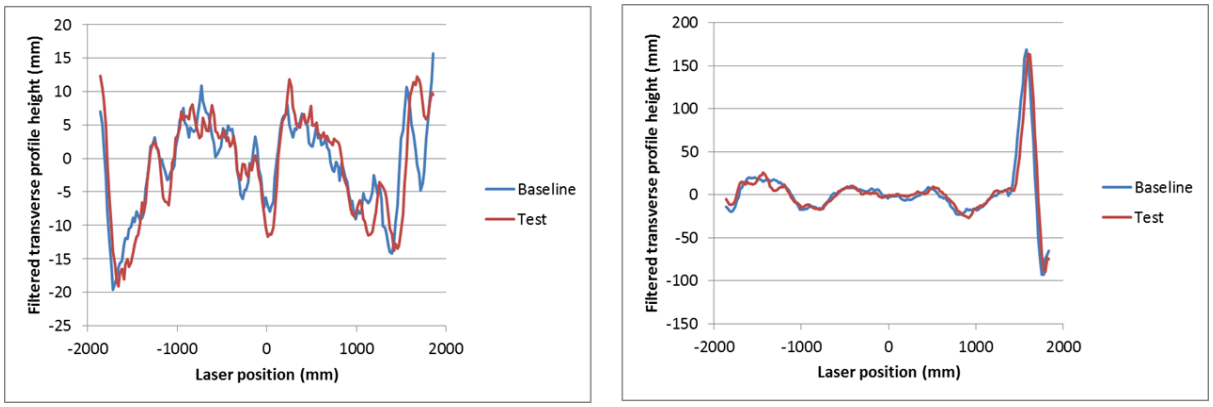

Figure 22: Baseline plotted against the test after removing long wavelengths and filtering to remove wavelengths less than 300mm

3.2.2.2 Correlation

The correlation value between the normalised test and baseline TPs is calculated. The test profile is then shifted slightly, and a new correlation value calculated. This process continues while the test profile moves through its range of possible positions. This produces a correlation curve showing how well the profiles are aligned throughout the range of tested alignment shifts. From this curve, the shift that corresponds to the maximum correlation (MC) value can be found, see Figure 23.

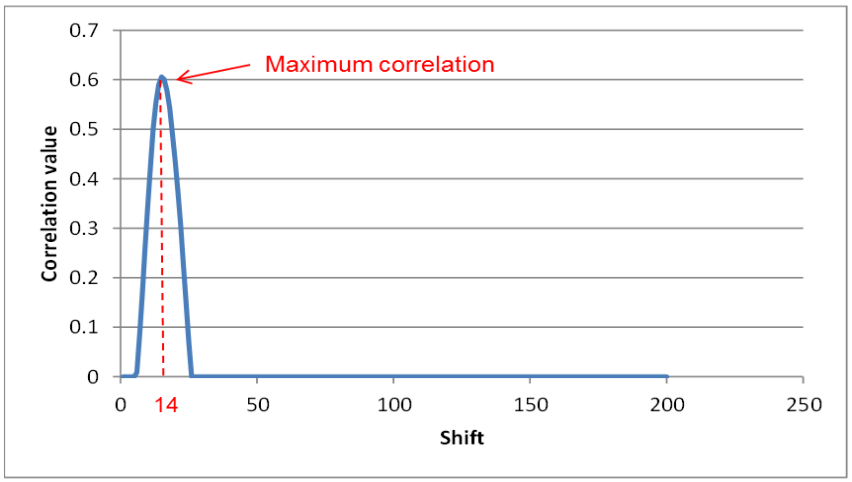

Figure 23: Example of a correlation curve showing correlation between test and baseline profiles with different profile alignment shifts.

The correlation curve shown in Figure 23 suggests that the test transverse profile should be transversally shifted by 14 sampling intervals in order to align it optimally with the baseline.

Figure 24 shows the baseline and test transverse profiles associated with the correlation curve depicted in Figure 23. The plot on the left shows the profiles before alignment, with the plot on the left showing the profiles following the transverse alignment process.

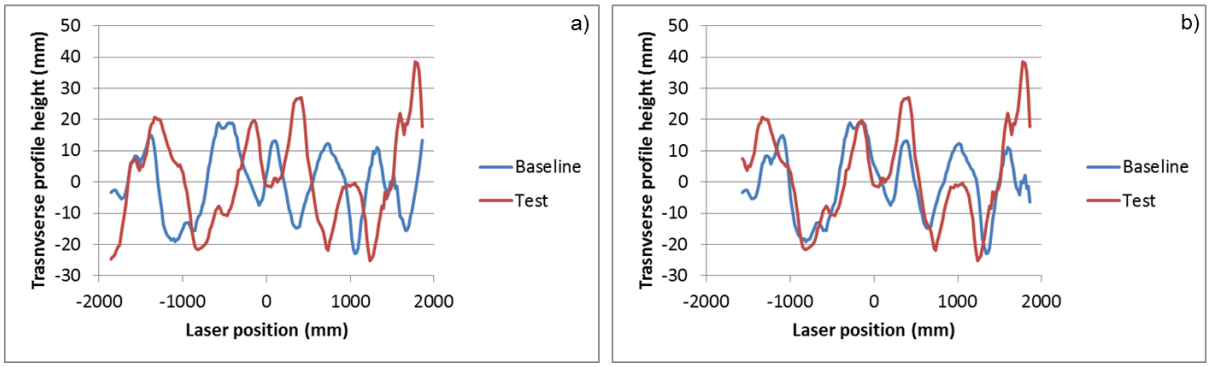

Figure 24: Illustration of the correlation results, a) Shape of the baseline and test for which the correlation curve in Figure 23 was calculated, b) Aligned baseline and test after applying a shift of 294mm

Figure 25 depicts the transverse shift values calculated, along the length of one of the test surveys. These were obtained using the maximum correlation method described above.

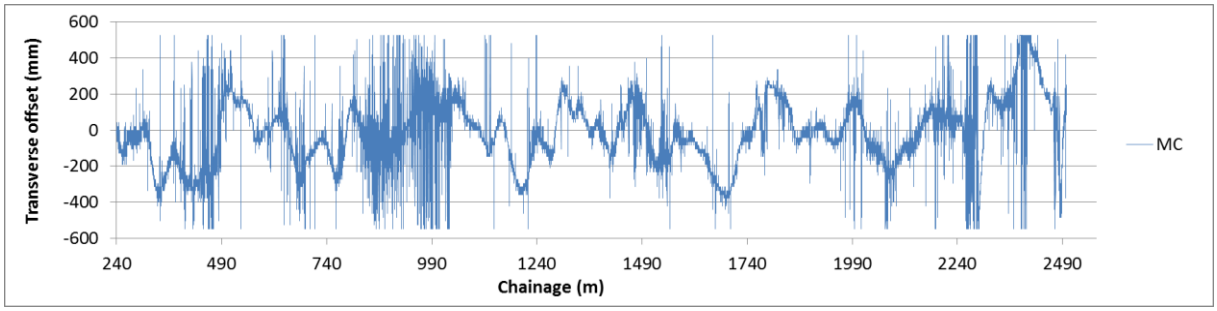

Figure 25: Transverse offset calculated based on the maximum correlation values

It is clear that there is a definite shape of the transverse shift curve with the appearance of a natural undulation, which is a result of variations in driving line. However, spikes and sudden large changes in the calculated shift factors can also be seen. These spikes are caused by the fact that the shift found using the maximum correlation values is not always correct if the correlation curve has several peaks. A series of decision rules was therefore introduced to reduce the occurrence of these spikes and logically inconsistent transverse shifts.

3.2.2.3 Defining the decision rule set

The decision rules are based on the assumption that such spikes cannot occur in natural driving, and must be smoothed out to avoid misaligning data.

The decision rules are built based on two cases; in the first case the sign of the spike is the same as the median of all the transverse offsets calculated over 1m before the occurrence of the spike; and in the second case, the sign of the spike is opposite to the sign of the median of the offsets in the 1m before the spike. The illustration of the occurrence of case 1 and case 2 is illustrated in Figure 26, showing a section located between 600m and 700m in test Run 1.

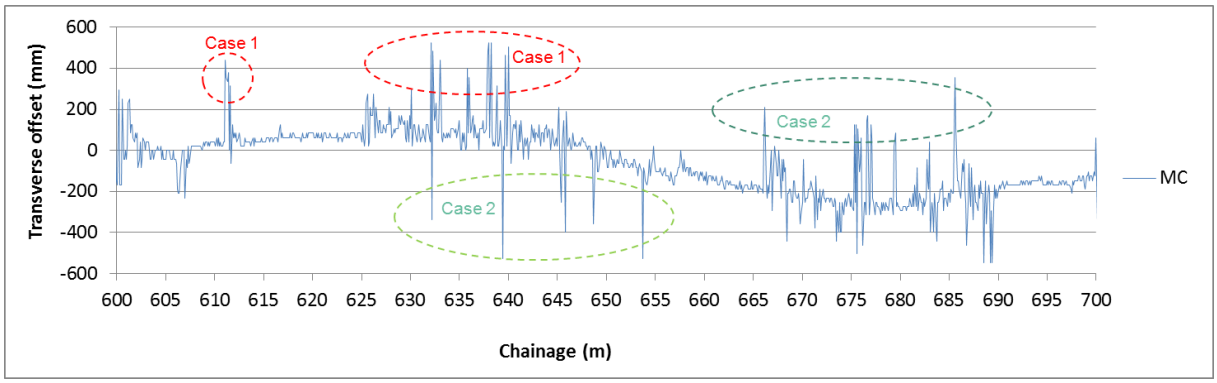

Figure 26: Illustration of case 1 where the sign of the spike is the same as the sign of the natural curve; and case 2 where the sign of the spike is opposite to the sign of the natural curve.

The decision rule algorithm is outlined in Figure 27. The algorithm classifies the peaks as being in either case1 or case2. When a spike is identified the algorithm then re-examines the correlation curve to identify additional correlation peaks. Then the algorithm locates all the correlation peaks that occurs in the first half of the correlation curve or the second half of the correlation curve; then computes the minimum shift or the maximum shift corresponding to the minimum or the maximum of all the correlation peaks in the first half or the second half. Figure 28, depicts the resulting curve (shown in red) after running the decision algorithm.

- Let the shift value based on the maximum correlation curve be S_{max}.
- Let the median of offset values calculated in the previous 1m be M
- Let Sgn be the sign function.
- TOL = 3.
- If Sgn(S_{max}) is the same as Sgn(M) then:
  - Split the correlation curve into two halves;
  - Let S_{min1} be the minimum shift of all the correlation peaks detected in the first half;
  - Let S_{min2} be the minimum shift of all the correlation peaks detected in the second half;
  - S_{min1} = M, if S_{min1}<M-TOL, or S_{min1} >=M +TOL;
  - S_{min2} = M, if S_{min2}<M-TOL, or S_{min2} >=M +TOL;
  - Use S_{min1} or S_{min2} as the new shift value depending on Sgn(M) positive or negative.
- If Sgn(S_{max}) is opposite to Sgn(M) then:
  - Split the correlation into two halves;
  - Let the shift value based on the maximum correlation in the first half be S_{max1};
  - Let the shift value based on the maximum correlation in the second half be S_{max2};
  - If S_{max}<0:
    - If S_{max}>M-TOL and S_{max}<M+TOL, use S_{max1} as the new shift value;
    - Otherwise use M as the new shift value.
  - If S_{max}>0,
    - If S_{max}>M-TOL and S_{max}<M+TOL use $-S_{max2}$ as the new shift value;
    - Otherwise use –M as the new shift value.

Figure 27: Decision algorithm to deal with anomalous offset values

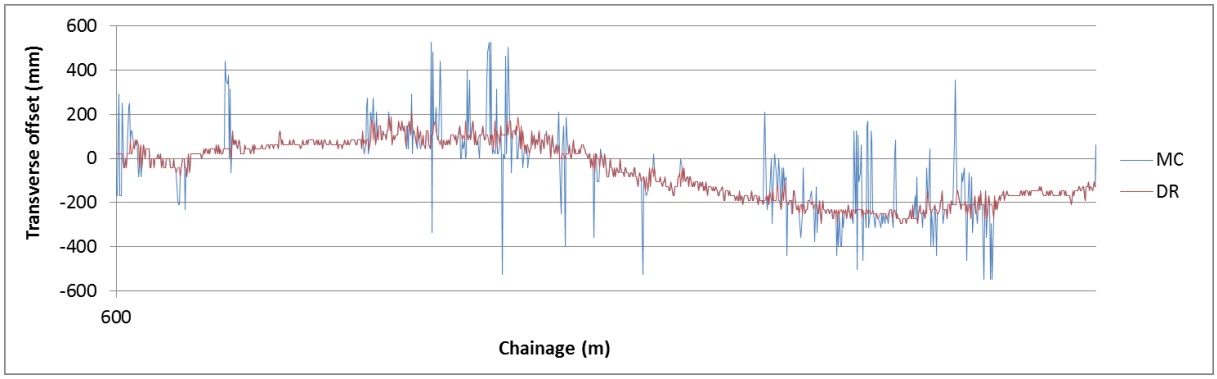

Figure 28: Application of the decision rule set to the remove spikes in Figure 26

The comparison of the transverse offset calculation for test Run 1, before and after the application of the DR algorithm is given in Figure 29, this illustrates that the removal of the spikes was successful for a larger data set, and has produced a much smoother set of transverse shifts, with far fewer unrealistic or illogical discontinuities in position.

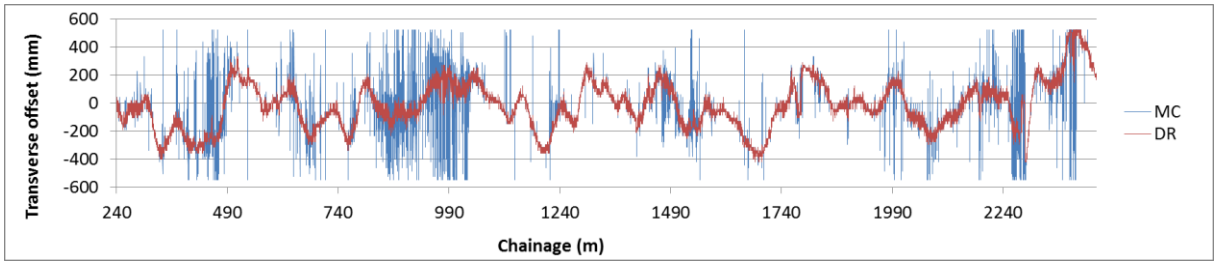

Figure 29: Comparing calculated transverse offset, for test Run 1, before and after applying the decision rule algorithm (DR) over the whole test site.

3.2.2.4 Smoothing based on the neighbourhood value

In addition to the alignment corrections obtained using the decision rules, a further stage of smoothing is applied to the calculated shift factors. The smoothing is based on the calculated shift values in the data from a region located 6m before and after the spike. In order to do this, a polynomial moving average with a half window of 6m is applied to the transverse offsets resulting from the application of the DR algorithm (this is the red curve labelled DR in Figure 29). For a given data point, the square of its deviation from the moving average is calculated. If this is greater than a specified threshold value (currently set to be equal to 5), the data point is deemed to be anomalous, and the transverse shift value at this location is replaced by the moving average value at that point. The red line in Figure 30 illustrates the additional smoothing obtained using this algorithm.

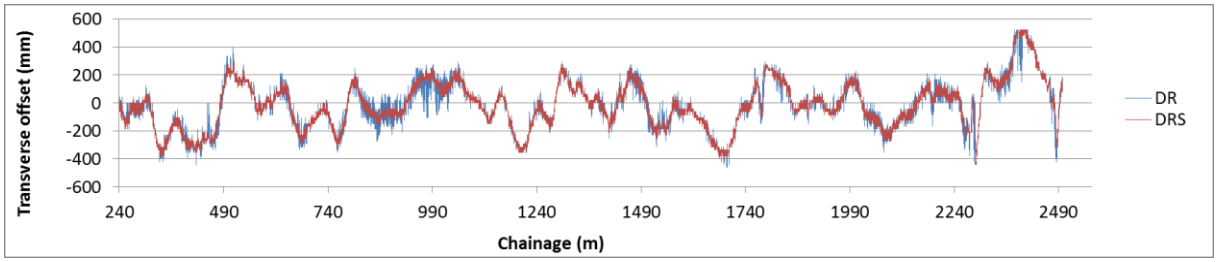

Figure 30: Comparing calculated transversal offset, for test Run 1, applying only the decision rule algorithm (DR) and applying DR and smoothing based on the neighbourhood values (DRS)

3.2.3 Validation of the alignment algorithm

The performance of the alignment algorithm was assessed by using the reference data created by manual analysis of the chalk line in the HARRIS2 images (Section 3.1.2). The calculated transverse and longitudinal shifts required to align each test data set with the baseline data were compared against the reference shifts.

The plots shown in Figure 31 show the calculated and reference transverse shifts for four of the test runs. The reference shifts are shown in a thick coloured line, with the calculated shifts shown as the thinner grey line.

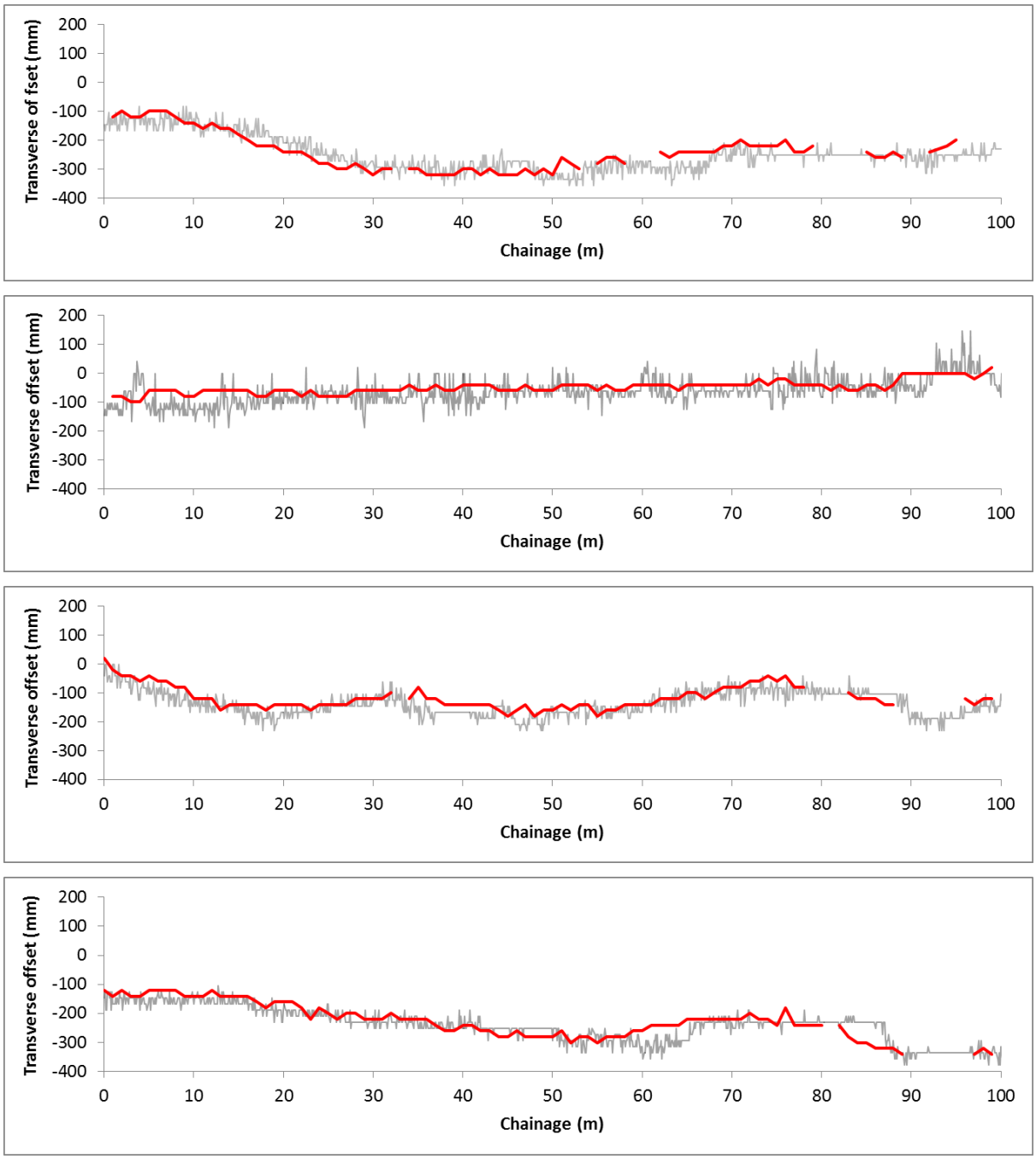

Figure 31: Comparison of the automatic alignment and the manual alignment for (from top) Run 1, 2, 3 and 4.

Overall the agreement between the reference and the calculated shifts from the automatic alignment is very good. There are small differences and the calculated shifts are seen to exhibit more high frequency variation. Some of this may be due to the fact that the reference shifts were only measured every 1m, whereas the calculated shifts were available every 100mm, some may be due to difficulties and inaccuracies in producing the reference data and identifying precisely which part of the marked line in each test run corresponded with each part of the marked line in the reference data, and some may be due to the level of detail used in the reference data (20mm grid cells in ChartCrack).

Table 2 shows the proportion of the test length with calculated transverse alignment shifts of greater than 100mm from measurement point to measurement point. Such large changes in transverse positioning of the survey vehicle are unlikely to be valid. The figures in the table show the proportions of calculated shifts of this magnitude or greater following the application of the initial, correlation based alignment process, and also with the Decision Rules applied to the alignment.

Table 3 shows the mean calculated transverse shift values for the four test runs discussed.

Table 2: Proportions of calculated transverse shifts in test length greater than 100mm in magnitude.

Test run	Correlation only	With Decision Rule set
1	21.5%	3.2%
2	15.2%	4.5%
3	18.4%	3.8%
4	23.2%	2.7%
Mean	**19.6%**	**3.6%**

Table 3: Mean calculated transverse shifts in test length.

Test run	Correlation only	With Decision Rule set
1	97.2 mm	25.9 mm
2	63.6 mm	28.9 mm
3	75.3 mm	26.0 mm
4	96.7 mm	22.1 mm
Mean	**83.2 mm**	**25.7 mm**

It can be clearly seen that, although there are still a small number of these unlikely large transverse shifts, the proportion of these is greatly reduced using the decision rules, as is the magnitude of the typical calculated alignment shift.

As well as reducing the number of unrealistic shifts, the algorithm output when the Decision Rules are implemented, also show smaller variation from the reference dx shifts, calculated by inspection. These reference shifts were calculated using a data resolution of 20mm transversally. Figure 32 shows the frequency distribution of the differences between the calculated and the reference dx shifts using only the correlation approach, and implementing the Decision Rules. These same data are shown in terms of the cumulative frequency of the absolute magnitude of the differences in the dx shifts in Figure 33.

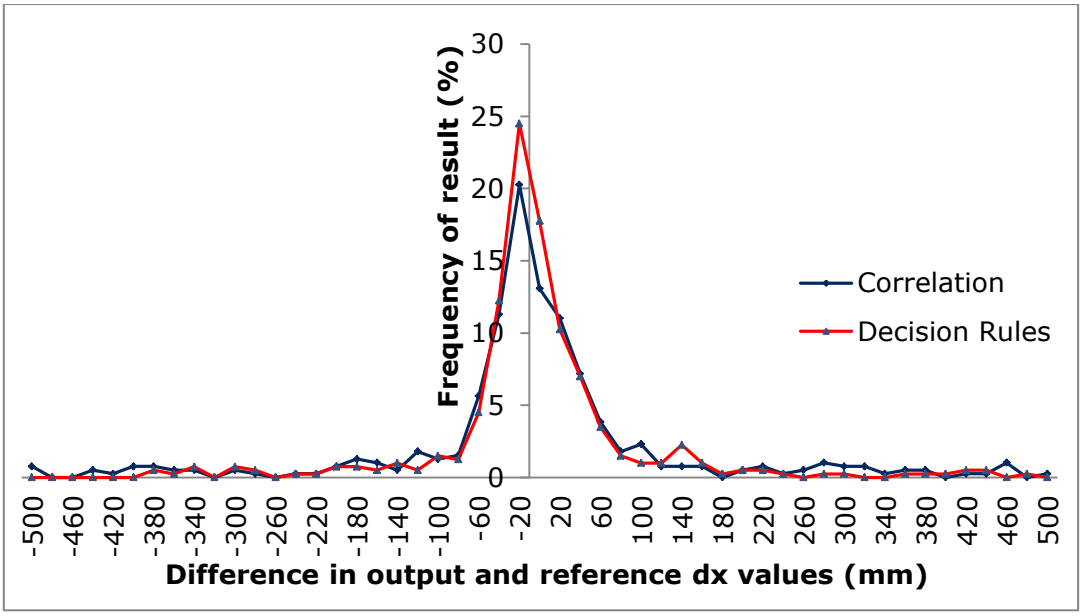

Figure 32: Distribution of variation between calculated and reference dx shifts using only the correlation approach, and by implementing the Decision Rules.

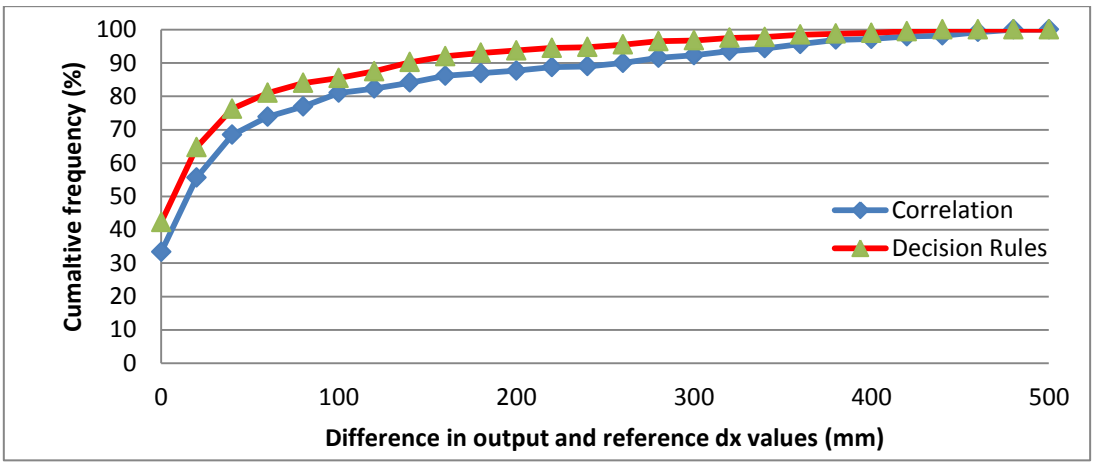

Figure 33: Cumulative distribution of the absolute magnitude of variation between calculated and reference dx shifts using only the correlation approach, and implementing the Decision Rules.

It can be seen that by implementing the Decision Rules, the calculated shifts in the profile positions are closer to those found by inspection in the reference data. Using the correlation approach alone puts 65% of data within ±40mm of its 'true' transverse position according to the reference data; with the Decision Rules in place, the performance improves such that 65% of calculated transverse shifts are now within ±20mm of the reference data.

4 Practical investigation on the effect of fretting on road surface shape

The aims of the experimental work were to identify how early signs of surface disintegration in laboratory samples manifest themselves in the measured surface shape, and determine whether parameters could be developed to characterise the shape and support the identification of surface disintegration. To commence this work initial investigations into potential sample creation and wear methods were undertaken, which then informed the decisions made in the main experimental work.

Initial investigations

A series of tests were conducted with a view to establishing suitable methods for producing surface disintegration on laboratory samples of pavement materials. The aim was to introduce surface disintegration to the samples and track the progression of this using high-resolution 3-D surface profile measurement data.

An initial test was carried out to identify a suitable tool to induce the surface disintegration, using four samples of SMA. Figure 34 shows samples SMA1 and SMA2. Figure 35 shows samples SMA3 and SMA4. All samples were made using the same batch mix of binder and aggregate using a standard mixture recipe. The samples were composed of approx. 10mm aggregate, grit-blasted to remove surface binder which was causing problems for the collection of 3-D data.

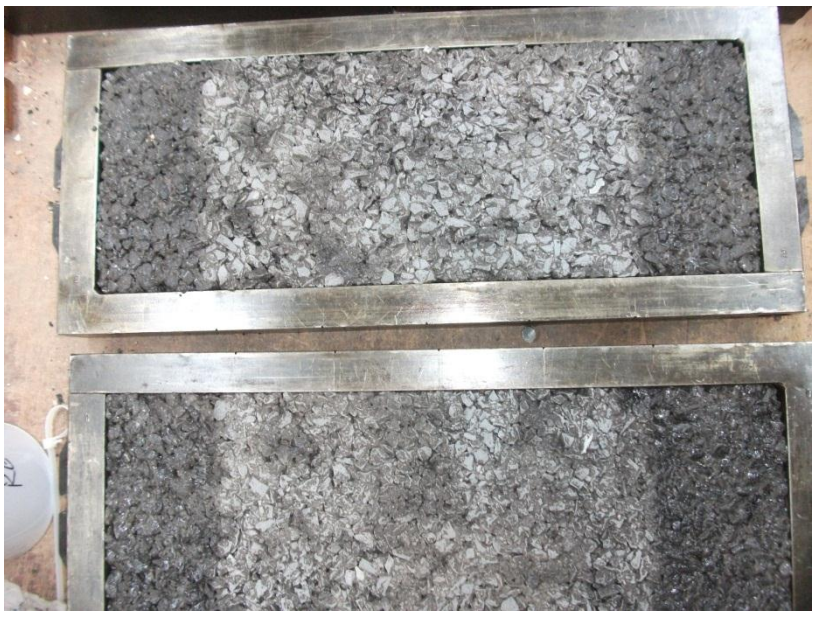

Figure 34: Samples SMA1 and SMA2

Figure 35: Samples SMA3 and SMA4

Two different machines and test methods were tested to see if they would produce fretting in the desired manner. These were the MLPC pavement Rutting Tester, and the Wheeltracker machine. Both approaches involved making multiple repeated passes of a weighted wheel over the surface being tested. It was possible to control the machine (and sample) temperature, the force being exerted on the surface by the wheel, the running angle of the wheel, and the number of passes.

The tests were deliberately done quite conservatively in order to avoid destruction of the samples before any useful data could be collected as the expected rate of deterioration which was produced was uncertain.

It was concluded that the wear produced by the MLPC rutting machine was more representative of the types of deterioration of interest in this research, although it was noted that the methodology did produce rutting in the early stages of wearing the samples, which was not unexpected, given the purpose and design of the machine used.

4.1 Experimental details and procedure

Based on the findings and experience of the initial investigation a series of laboratory samples were made, and subjected to forced wear and deterioration.

4.1.1 Samples

Test samples were produced using (6mm) aggregate, to enable fine changes to take place and give more range to the measurements, and were created with slightly different mixes of bitumen than the samples used in the initial investigation. One of the samples (slab5) was a standard, good quality mix with 6mm aggregate, the other (slab6) used the same aggregate, but the binder had 50% bitumen content.

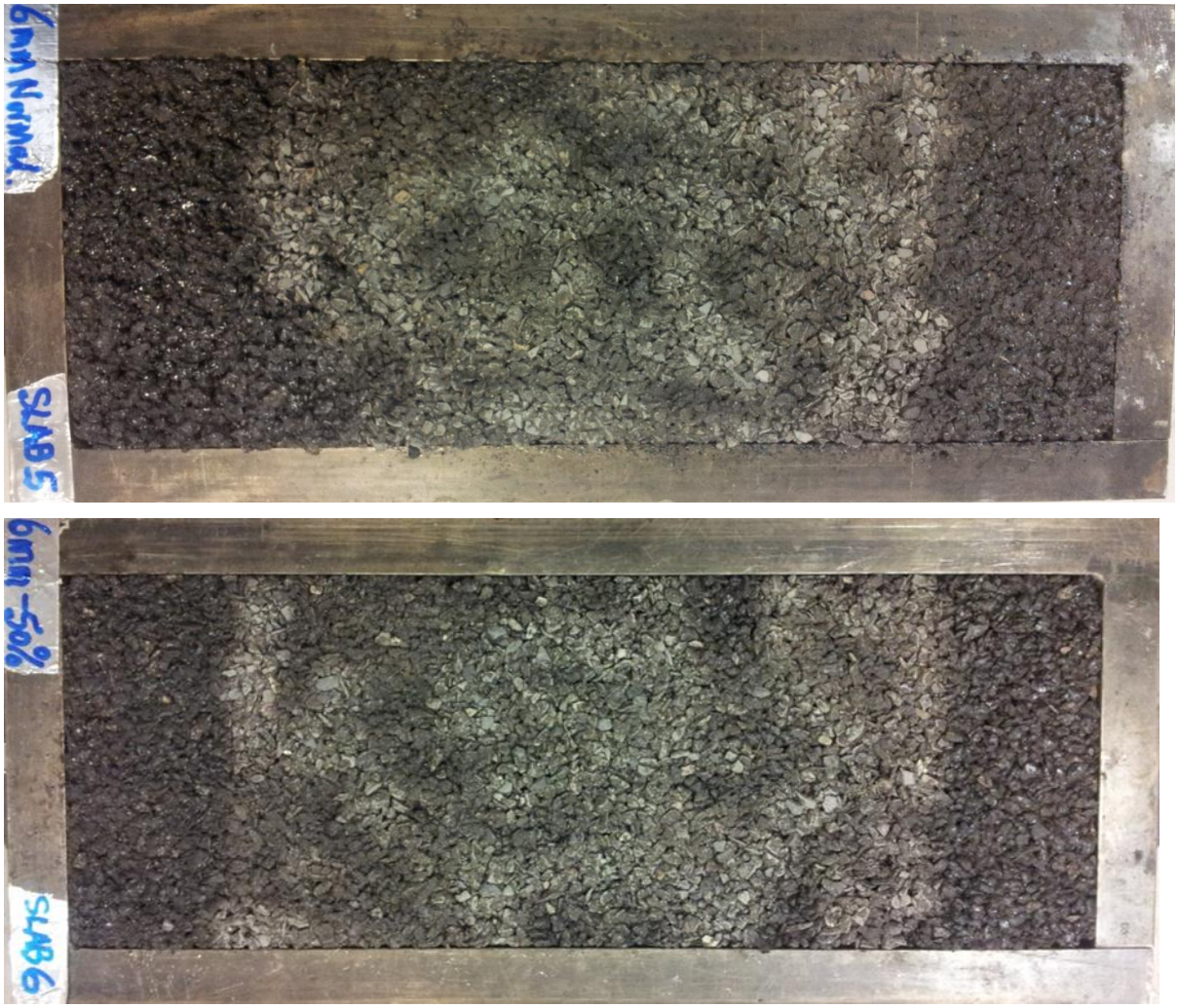

Figure 36: Samples used in laboratory testing. Light area in middle of samples has been grit blasted to remove surface bitumen and improve Breuckmann data collection by reducing reflections.

4.1.2 Wearing

As noted above, the MLPC rutting tester was identified in the initial testing as being the best method available for use within the project to produce simulated surface disintegration. However to increase the friction and reduce the rolling of the wheel, the angle at which the wheel moved relative to the axis of rotation was increased from 5° to 10°.

Figure 37: Sample in place in MLPC rutting machine for wearing.

The samples were tested side by side in the MLPC rutting machine at ambient temperature. Testing was carried out at ambient temperature in an effort to minimise the rutting produced by the machine.

The settings used in the tests with the MLPC machine are as shown in Table 4.

Table 4: Settings used in MLPC Pavement Rutting Tester

Wheel running angle	10°
Temperature of machine and sample	Ambient (between 18 – 25°C)
Force applied	2000N

4.1.3 Surface shape measurement

The Breuckmann smartSCAN system was used to collect 3-D data on each sample before any trafficking had taken place, after every 1000 wheelpasses in the MLPC machine, and repeatedly following the completion of the wearing process after 25000 passes.

Figure 38 shows one of the samples being imaged using the Breuckmann system. The pattern visible is the projected light used in the calculation of the surface shape.

Samples were placed on the floor in front of the Breuckmann system, within the optimum imaging zone (approximately 1.5m from the sensors. The samples were not moved or rotated during the imaging process, but the camera was oriented to maximise

the data obtainable from a single position. This involved making measurements from above at an angle of between 20° and 30° from vertical.

The data collection and processing prior to export was controlled using the Breuckmann OptoCat software. The software was used to control the camera and system settings such as the exposure time and data resolution. If multiple scans were required in order to correctly record data on both the dark and light parts of the surface then these were merged and a single surface was created using data from all available scans. Once the scan data and parameters were saved the surface was exported as a mesh file. This was suitable for import into MountainsMap Universal, the surface analysis software which was used to inspect the measured data and extract parameters and measurements (see Section 4.1.4). The Breuckmann SmartSCAN system was set up to collect data at the full resolution (pixel resolution of 0.444mm, using 4 separate collections, in which the exposure time settings were adjusted to optimise the recording of data on both the dark and lighter parts of the sample. Measurements were made of the sample using exposures of 500, 300, 150 and 68ms). To avoid problems with noise and spurious datapoints an averaging window of 8 pixels was used. Following data collection the 4 scans were merged to produce a single model of the surface, and then exported as an ASCII file containing the x,y,z coordinates of each point in the data. Holes in the data were filled using MountainsMap, and parts of the dataset which were of no interest were removed to leave only the sample surface.

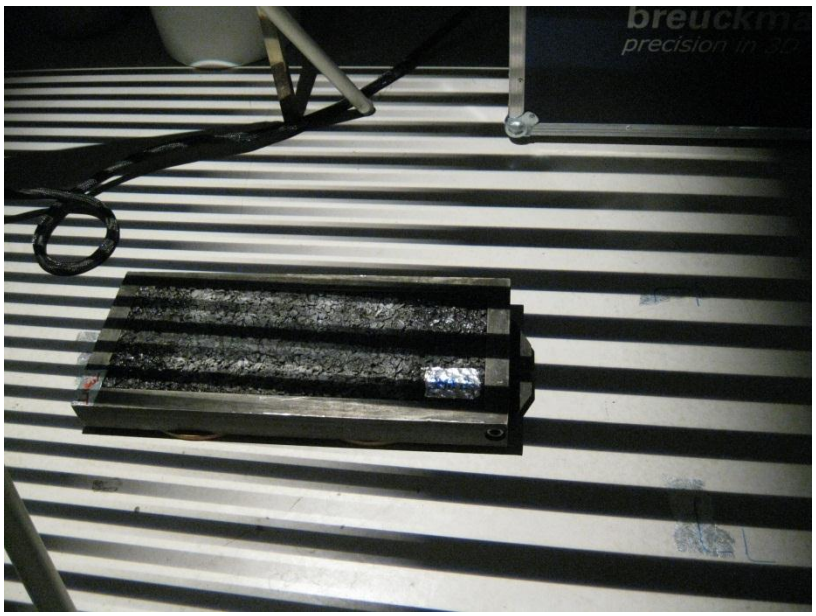

Figure 38: Sample being imaged using Breuckmann camera showing one of the structured light patterns

After 25,000 passes the difference in deterioration is obvious to the naked eye, and locations where aggregate chips have been removed are identifiable (see photos in Figure 39 and Figure 40).

Figure 39: Photograph of slab 5 after 0 passes

Figure 40: Photograph of slab 5 after 25000 passes

Examples of the 3-D measured surface models created using the data from the Breuckmann SmartSCAN camera are shown in Figure 41 and Figure 42. These show the same slab, in the same orientation as shown in Figure 39 and Figure 40.

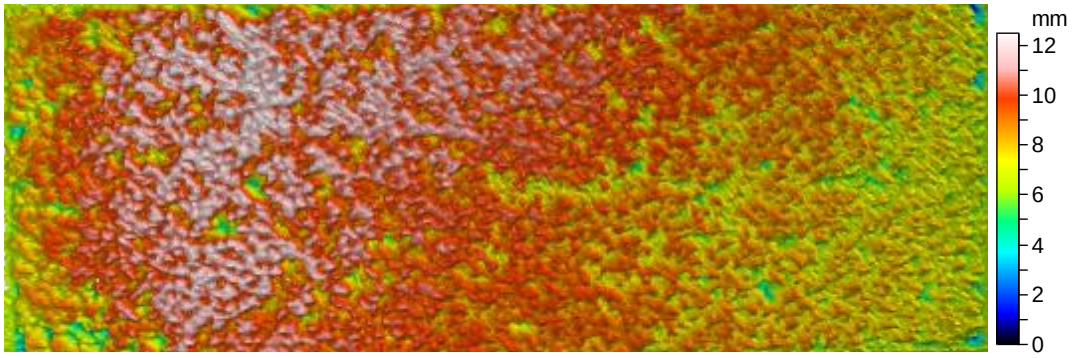

Figure 41: 3-D model of slab 5 after 0 passes

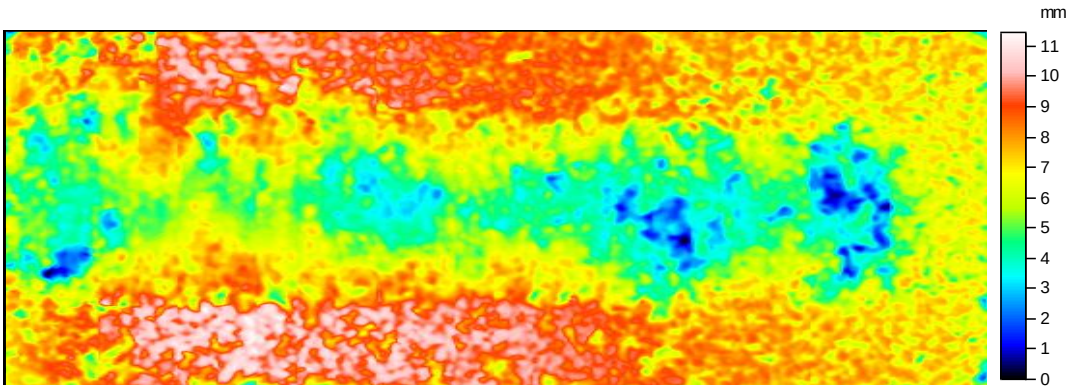

Figure 42: 3-D model of slab 5 after 25000 passes

In the following sections we try to evaluate if the 3D camera can be used to detect signs of surface deterioration. The research question posed was:

- **If the change in surface as it was trafficked could be detected by the data, then which of the parameters measured detect this change the best?**

4.1.4 Parameter extraction

MountainsMap Universal © software was used to process the collected data and extract potential parameters to characterise the shape of the pavement sample. For the data extraction process the surface was considered as a series of individual grid cells (50 mm x 50 mm squares), and parameters of interest were extracted for each cell, after each 1000 passes.

The cells were chosen to be non-overlapping, and to avoid issues with boundary effects. A narrow region between the region of interest and the edge of the sample was excluded to avoid including the metal frame in the data. The non-overlapping nature of the cells was also designed to assist with subsequent linear regression analysis into parameters and their relationship to condition change.

The cells were specifically chosen to lie in three rows (Figure 43). The nature of the accelerated wear method chosen meant that almost all of the effects of the trafficking were confined to the middle row of the sample, while the top and bottom cells were hardly trafficked at all. This meant that the resulting data from the top and bottom cells should not be affected by changes in condition, while the middle row should reflect the trafficking.

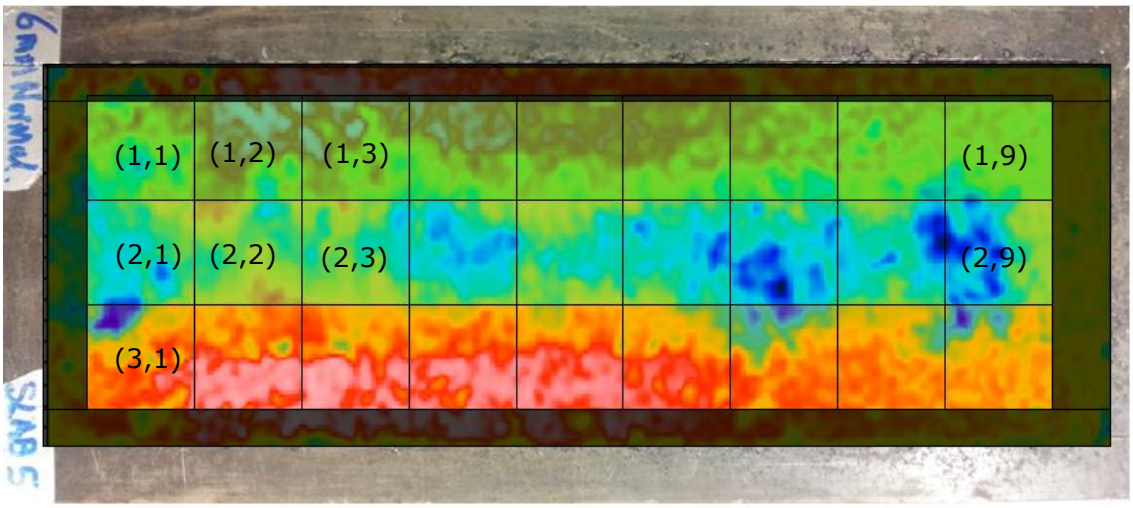

Figure 43: Illustration of parameter extraction cells overlaid on 3-D model produced by MountainsMap using Breuckmann data.

Figure 44 provides a summary of the data collection, and parameter extraction workflow used to obtain data for further analysis. Thirty parameters were extracted based on calculations of the properties of the data at the full resolution available, and also at 1mm, 2mm, 5mm and 10mm resolutions. All extracted parameters are listed in the figure shown in Figure 46, and the shortlisted parameters used in the final analysis are presented in Table 5.

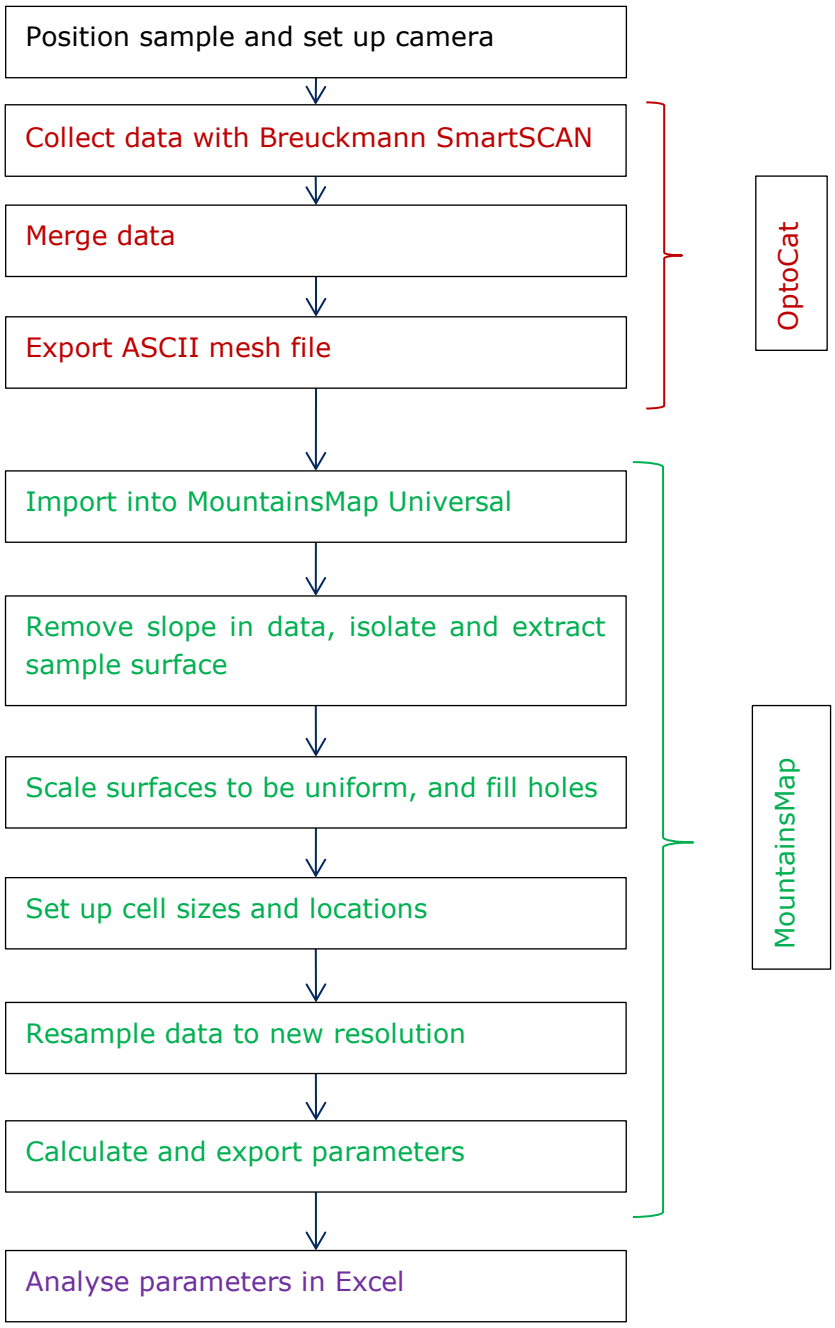

Figure 44: Data collection workflow

Many of the parameters of interest are related to the Abbot-Firestone curve (Jiang, Scott, Whitehouse, & Blunt, 2007), which is often used in characterising and understanding the properties of surfaces. The Abbott-Firestone curve is the cumulative probability density of the surface height measurements. Figure 45 illustrates some of the concepts useful in working with and understanding the Abbott-Firestone curve.

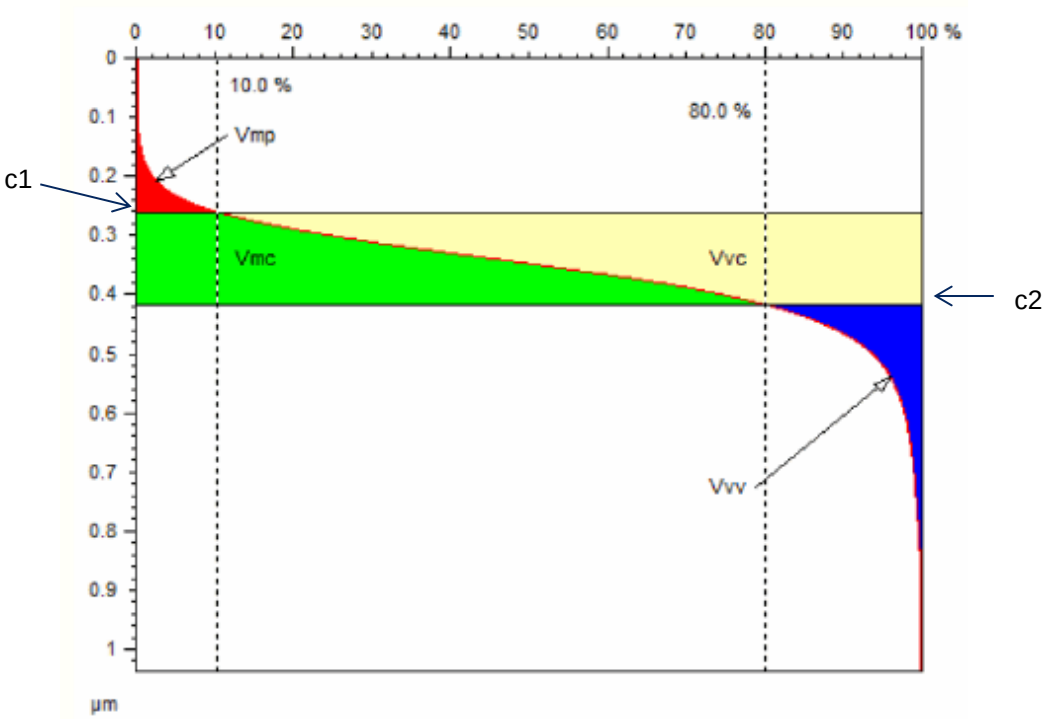

Figure 45: Abbott-Firestone curve

The curve is based on how much of a surface would be in contact with an intersecting plane at all heights from the highest peak to the lowest valley. This can be used to characterise and distinguish different surfaces. In the figure shown above, Vmp shows the volume of the surface in the peaks above height c1, Vmc shows the volume of the mass of the sample between heights c1 and c2, and Vvv shows the volume of the voids in the valleys below height c2 (the lowest parts of the sample). Typically c1 and c2 are set to be at the 10% and 80% levels respectively, although these can be changed. Changes in the surface condition of a sample are often reflected by changes in the shape of the associated Abbott-Firestone curve, and the parameters extracted from it. One of the limitations of the Abbott-Firestone curve is that it provides no spatial information about the distribution of different heights within a sample, but this is not necessarily a problem for this application if the survey data from successive sampling intervals is accurately aligned, and the parameters are extracted over small areas. The use of small 50mm square cells in the data processing and extraction means that although we do not know details about how the surface profile changes within that small area, we can characterise the overall surface using the data extracted from these small cells.

An initial sift of the parameters was carried out to eliminate any which were highly correlated with other parameters. Figure 46 shows how the parameters correlated with each other – red cells indicate parameters which were highly correlated, green cells show parameters which were uncorrelated. These were chosen for elimination because statistical methods such as multiple linear regression do not perform well with highly correlated variables. Additionally, some of the parameters were eliminated as they did not make conceptual sense in terms of the types of deterioration which were being investigated.

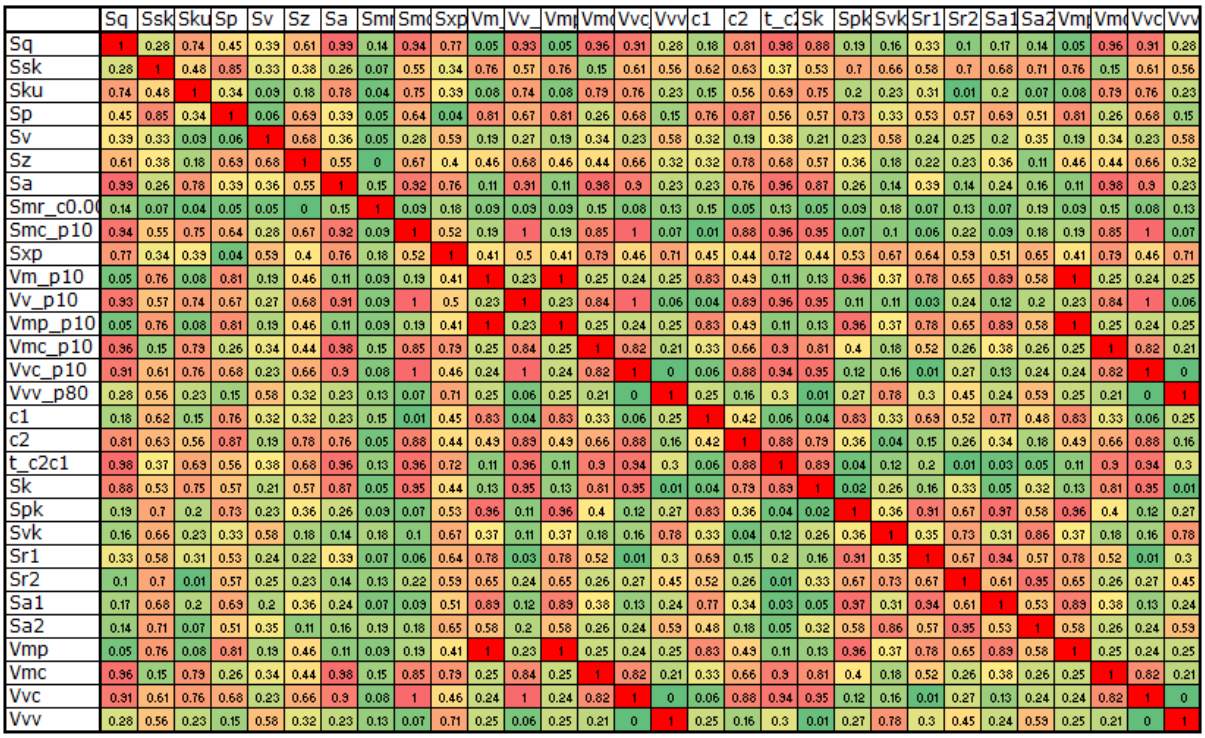

	Sq	Ssk	Sku	Sp	Sv	Sz	Sa	Smr	Smc	Sxp	Vm_	Vv_	Vmp	Vmc	Vvc	Vvv	c1	c2	t_c2	Sk	Spk	Svk	Sr1	Sr2	Sa1	Sa2	Vmp	Vmc	Vvc	Vvv
Sq	1	0.28	0.74	0.45	0.39	0.61	0.99	0.14	0.34	0.77	0.05	0.93	0.05	0.96	0.91	0.28	0.18	0.81	0.98	0.88	0.19	0.16	0.33	0.1	0.17	0.14	0.05	0.96	0.91	0.28
Ssk	0.28	1	0.48	0.85	0.33	0.38	0.26	0.07	0.55	0.34	0.76	0.57	0.76	0.15	0.61	0.56	0.62	0.63	0.37	0.53	0.7	0.66	0.58	0.7	0.68	0.71	0.76	0.15	0.61	0.56
Sku	0.74	0.48	1	0.34	0.09	0.18	0.78	0.04	0.75	0.39	0.08	0.74	0.08	0.79	0.76	0.23	0.15	0.56	0.69	0.75	0.2	0.23	0.31	0.01	0.2	0.07	0.08	0.79	0.76	0.23
Sp	0.45	0.85	0.34	1	0.06	0.69	0.39	0.05	0.64	0.04	0.81	0.67	0.81	0.26	0.68	0.15	0.76	0.87	0.56	0.57	0.73	0.33	0.53	0.57	0.69	0.51	0.81	0.26	0.68	0.15
Sv	0.39	0.33	0.09	0.06	1	0.68	0.36	0.05	0.28	0.59	0.19	0.27	0.19	0.34	0.23	0.58	0.32	0.19	0.38	0.21	0.23	0.58	0.24	0.25	0.2	0.35	0.19	0.34	0.23	0.58
Sz	0.61	0.38	0.18	0.69	0.68	1	0.55	0	0.67	0.4	0.46	0.68	0.46	0.44	0.66	0.32	0.32	0.78	0.68	0.57	0.36	0.18	0.22	0.23	0.36	0.11	0.46	0.44	0.66	0.32
Sa	0.99	0.26	0.78	0.39	0.36	0.55	1	0.15	0.92	0.76	0.11	0.91	0.11	0.98	0.9	0.23	0.23	0.76	0.96	0.87	0.26	0.14	0.39	0.14	0.24	0.16	0.11	0.98	0.9	0.23
Smr_c0.0	0.14	0.07	0.04	0.05	0.05	0	0.15	1	0.09	0.18	0.09	0.09	0.09	0.15	0.08	0.13	0.15	0.05	0.13	0.05	0.09	0.18	0.07	0.13	0.07	0.19	0.09	0.15	0.08	0.13
Smc_p10	0.94	0.55	0.75	0.64	0.28	0.67	0.92	0.09	1	0.52	0.19	1	0.19	0.85	1	0.07	0.01	0.88	0.96	0.95	0.07	0.1	0.06	0.22	0.09	0.18	0.19	0.85	1	0.07
Sxp	0.77	0.34	0.39	0.04	0.59	0.4	0.76	0.18	0.52	1	0.41	0.5	0.41	0.79	0.46	0.71	0.45	0.44	0.72	0.44	0.53	0.67	0.64	0.59	0.51	0.65	0.41	0.79	0.46	0.71
Vm_p10	0.05	0.76	0.08	0.81	0.19	0.46	0.11	0.09	0.19	0.41	1	0.23	1	0.25	0.24	0.25	0.83	0.49	0.11	0.13	0.96	0.37	0.78	0.65	0.89	0.58	1	0.25	0.24	0.25
Vv_p10	0.93	0.57	0.74	0.67	0.27	0.68	0.91	0.09	1	0.5	0.23	1	0.23	0.84	1	0.06	0.04	0.89	0.96	0.95	0.11	0.11	0.03	0.24	0.12	0.2	0.23	0.84	1	0.06
Vmp_p10	0.05	0.76	0.08	0.81	0.19	0.46	0.11	0.09	0.19	0.41	1	0.23	1	0.25	0.24	0.25	0.83	0.49	0.11	0.13	0.96	0.37	0.78	0.65	0.89	0.58	1	0.25	0.24	0.25
Vmc_p10	0.96	0.15	0.79	0.26	0.34	0.44	0.98	0.15	0.85	0.79	0.25	0.84	0.25	1	0.82	0.21	0.33	0.66	0.9	0.81	0.4	0.18	0.52	0.26	0.38	0.26	0.25	1	0.82	0.21
Vvc_p10	0.91	0.61	0.76	0.68	0.23	0.66	0.9	0.08	1	0.46	0.24	1	0.24	0.82	1	0	0.06	0.88	0.94	0.95	0.12	0.16	0.01	0.27	0.13	0.24	0.24	0.82	1	0
Vvv_p80	0.28	0.56	0.23	0.15	0.58	0.32	0.23	0.13	0.07	0.71	0.25	0.06	0.25	0.21	0	1	0.25	0.16	0.3	0.01	0.27	0.78	0.3	0.45	0.24	0.59	0.25	0.21	0	1
c1	0.18	0.62	0.15	0.76	0.32	0.32	0.23	0.15	0.01	0.45	0.83	0.04	0.83	0.33	0.06	0.25	1	0.42	0.06	0.04	0.83	0.33	0.69	0.52	0.77	0.48	0.83	0.33	0.06	0.25
c2	0.81	0.63	0.56	0.87	0.19	0.78	0.76	0.05	0.88	0.44	0.49	0.89	0.49	0.66	0.88	0.16	0.42	1	0.88	0.79	0.36	0.04	0.15	0.26	0.34	0.18	0.49	0.66	0.88	0.16
t_c2c1	0.98	0.37	0.69	0.56	0.38	0.68	0.96	0.13	0.96	0.72	0.11	0.96	0.11	0.9	0.94	0.3	0.06	0.88	1	0.89	0.04	0.12	0.2	0.01	0.03	0.05	0.11	0.9	0.94	0.3
Sk	0.88	0.53	0.75	0.57	0.21	0.57	0.87	0.05	0.95	0.44	0.13	0.95	0.13	0.81	0.95	0.01	0.04	0.79	0.89	1	0.02	0.26	0.16	0.33	0.05	0.32	0.13	0.81	0.95	0.01
Spk	0.19	0.7	0.2	0.73	0.23	0.36	0.26	0.09	0.07	0.53	0.96	0.11	0.96	0.4	0.12	0.27	0.83	0.36	0.04	0.02	1	0.36	0.91	0.67	0.97	0.58	0.96	0.4	0.12	0.27
Svk	0.16	0.66	0.23	0.33	0.58	0.18	0.14	0.18	0.1	0.67	0.37	0.11	0.37	0.18	0.16	0.78	0.33	0.04	0.12	0.26	0.36	1	0.35	0.73	0.31	0.86	0.37	0.18	0.16	0.78
Sr1	0.33	0.58	0.31	0.53	0.24	0.22	0.39	0.07	0.06	0.64	0.78	0.03	0.78	0.52	0.01	0.3	0.69	0.15	0.2	0.16	0.91	0.35	1	0.67	0.94	0.57	0.78	0.52	0.01	0.3
Sr2	0.1	0.7	0.01	0.57	0.25	0.23	0.14	0.13	0.22	0.59	0.65	0.24	0.65	0.26	0.27	0.45	0.52	0.26	0.01	0.33	0.67	0.73	0.67	1	0.61	0.95	0.65	0.26	0.27	0.45
Sa1	0.17	0.68	0.2	0.69	0.2	0.36	0.24	0.07	0.09	0.51	0.89	0.12	0.89	0.38	0.13	0.24	0.77	0.34	0.03	0.05	0.97	0.31	0.94	0.61	1	0.53	0.89	0.38	0.13	0.24
Sa2	0.14	0.71	0.07	0.51	0.35	0.11	0.16	0.19	0.18	0.65	0.58	0.2	0.58	0.26	0.24	0.59	0.48	0.18	0.05	0.32	0.58	0.86	0.57	0.95	0.53	1	0.58	0.26	0.24	0.59
Vmp	0.05	0.76	0.08	0.81	0.19	0.46	0.11	0.09	0.19	0.41	1	0.23	1	0.25	0.24	0.25	0.83	0.49	0.11	0.13	0.96	0.37	0.78	0.65	0.89	0.58	1	0.25	0.24	0.25
Vmc	0.96	0.15	0.79	0.26	0.34	0.44	0.98	0.15	0.85	0.79	0.25	0.84	0.25	1	0.82	0.21	0.33	0.66	0.9	0.81	0.4	0.18	0.52	0.26	0.38	0.26	0.25	1	0.82	0.21
Vvc	0.91	0.61	0.76	0.68	0.23	0.66	0.9	0.08	1	0.46	0.24	1	0.24	0.82	1	0	0.06	0.88	0.94	0.95	0.12	0.16	0.01	0.27	0.13	0.24	0.24	0.82	1	0
Vvv	0.28	0.56	0.23	0.15	0.58	0.32	0.23	0.13	0.07	0.71	0.25	0.06	0.25	0.21	0	1	0.25	0.16	0.3	0.01	0.27	0.78	0.3	0.45	0.24	0.59	0.25	0.21	0	1

Figure 46: Parameter correlations

This left a list of seven parameters to be studied further (Table 5):

Table 5: Parameters used in analysis

Parameter name	Description
c1	Profile height defining volume in peaks – set to include top 10% by default.
c2	Profile height defining volume in valleys – set to include lowest 20% by default.
Vmp	Peak material volume of scale limited surface: Volume of material in the peaks of the sample, between 0% material ratio and material ratio p%, calculated in the zone above c1 $Vmp = \frac{K}{100\%}\int_{p}^{100\%}[Smc(p) - Smc(q)]dq$ Where K is a constant.
Vmc	Core material volume of the scale limited surface: Volume of material in the core, between two material ratios p and q, calculated in the zone between c1 and c2. Vmc = Vm(q) – Vm(p)
Sp	Maximum peak height.
Sr1	Upper material ratio.
Sr2	Lower material ratio.

4.1.5 Reference data

Producing reference data for the condition of the samples as the wear process proved to be very difficult. The small size and unnatural appearance of the samples made it difficult to undertake any visual assessment of the surfaces as inspectors are used to considering pavement condition over areas significantly larger than the total sample size. It was still possible to perform some visual condition monitoring on the samples, for example the point at which particular stones were removed from the surface could be detected, but these condition assessments are of specific events, and were not as indicative of changes that take place on network roads as we wanted, and were hard to use in any quantitative analysis.

An alternative approach of weighing the samples before trafficking commenced, and at each data collection break (after each 1000 passes) was proposed. The idea behind this was that the loss of surface material would be linked to the deterioration of the surface, and that this would be reflected in the measured weight. Unfortunately none of the available scales was able to both cope with the weight of the samples, and also report measurements at a fine enough resolution.

The only unambiguous quantitative measure which remained which may have been linked to the condition of the surface was the number of passes which the sample had been subjected to, and consequently this was used to help assess the ability of the extracted parameters to report the condition of the surfaces as deterioration progressed.

4.2 Use of 3-D parameters for detecting surface disintegration

4.2.1 Parameter behaviour

In assessing the extracted surface parameters it was noticed that the measurements made in the trafficked cells often tended to exhibit rapid changes in value over the first 1000 wheelpasses.

This initial rapid change is likely to be due to additional compaction of the sample material, and the initial polishing of the surface and removal of surface bitumen. In order to remove these effects it was decided to exclude measurements made until the sample had undergone 4000 passes, by which time these initial rapid changes had stabilised, and the changes in parameters would be more likely to reflect aggregate loss, or the small changes prior to aggregate chippings being removed from the surface of the sample.

These rapid initial changes are illustrated in Figure 47, which shows a single parameter for the first 5000 wheelpasses, and can also be seen in the full plots of all extracted parameters shown in Figure 48. In these plots, data from trafficked cells are shown in red, while the non-trafficked cells are shown in green and blue.

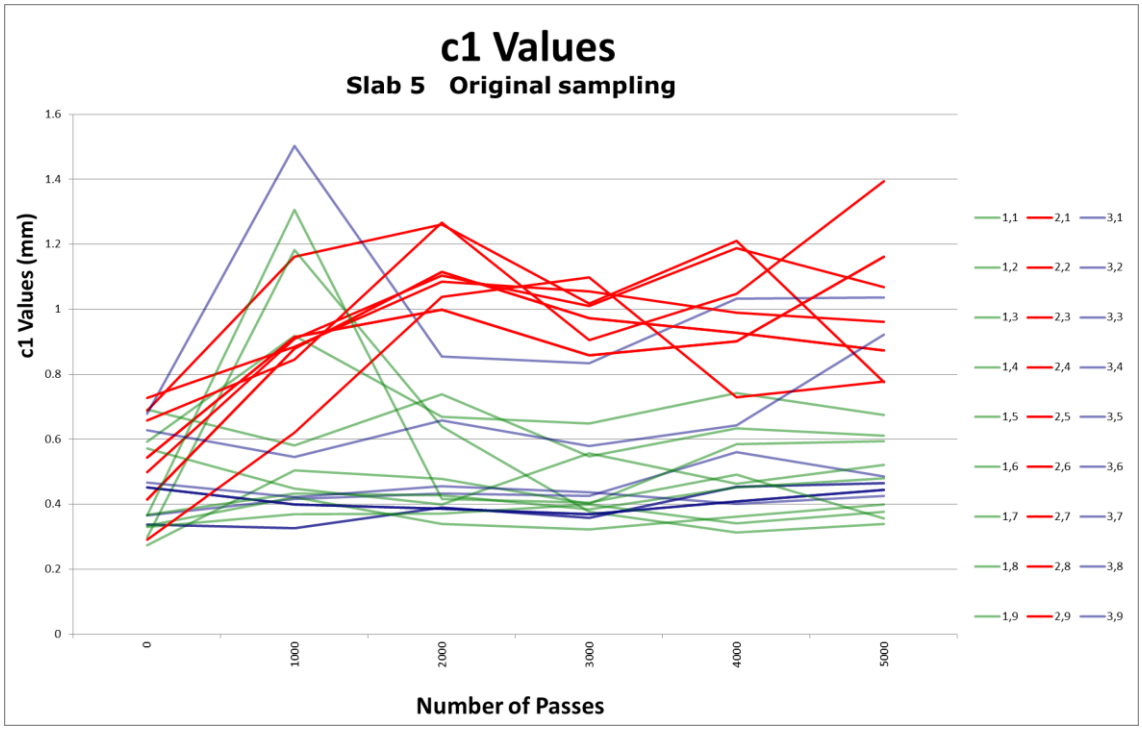

Figure 47: Example of rapid changes during initial trafficking of slab5.

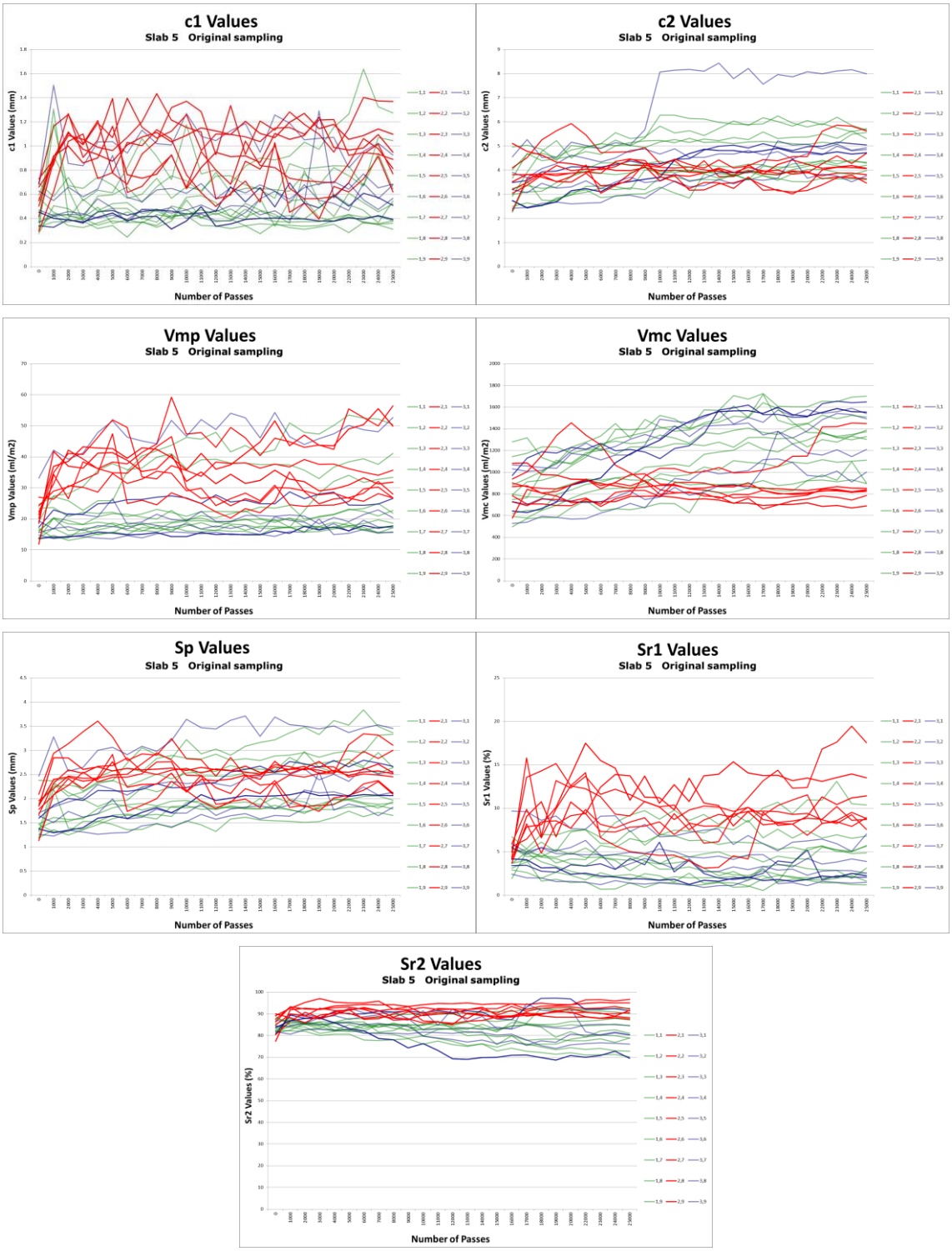

Figure 48: Values of extracted parameters, extracted from each cell on Slab 5, after every 1000 passes. Red lines show trafficked cells, blue and green lines show values from un-trafficked cells.

4.2.2 Use of parameters to detect absolute condition

To determine if a difference could be observed in any of the seven parameters between the trafficked and non-trafficked cells as the levels of wear increased the behaviour of the parameters were investigated. The graphs in Figure 49 show the mean value for each parameter across the nine trafficked cells and 18 non-trafficked cells of slab5 (ignoring the first 3000 passes).

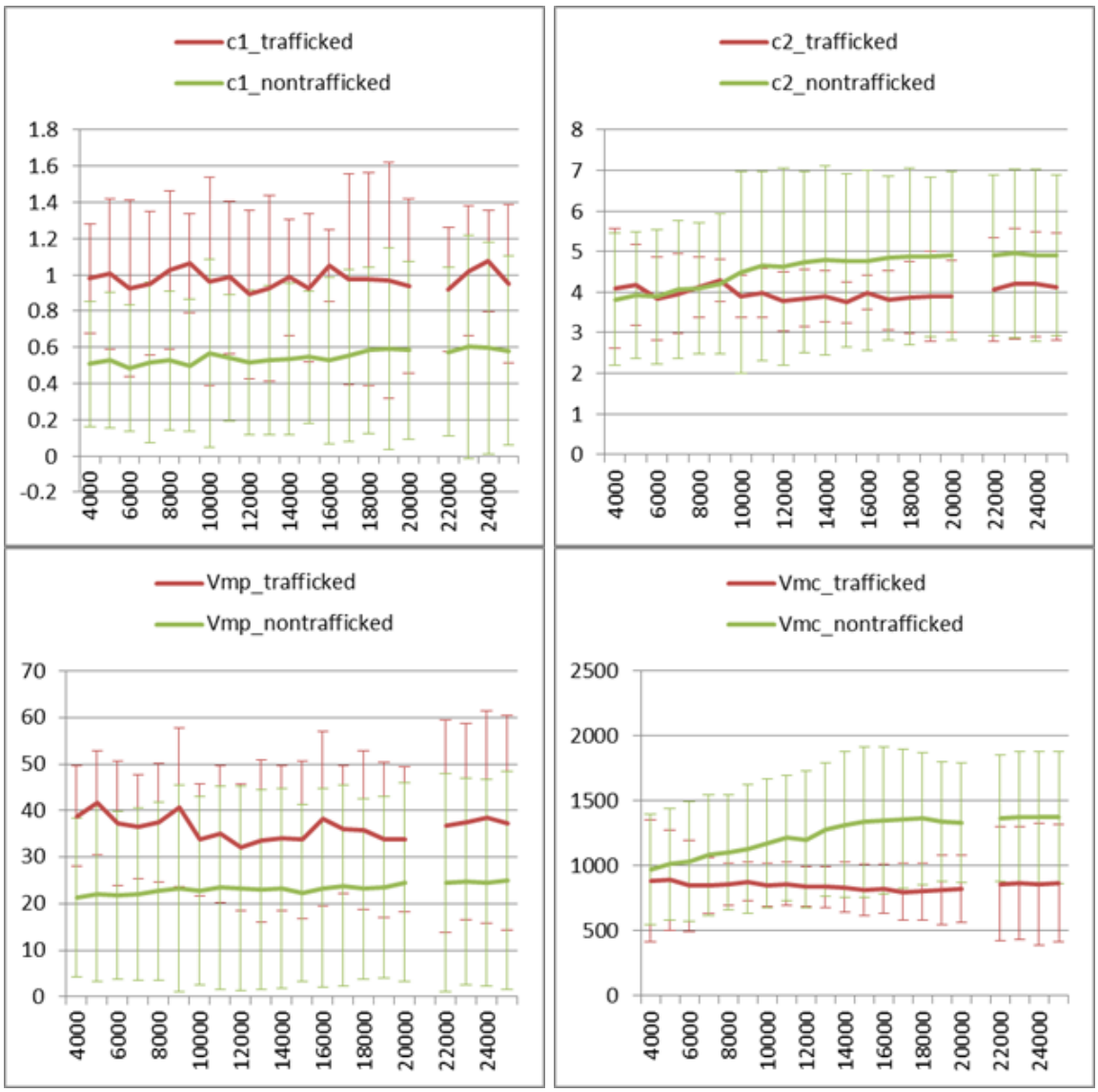

Figure 49: Mean trafficked and non-trafficked measurement for each parameter (slab 5)

The error bars display +/- two standard deviations; this represents the range in which approximately 90-98% of the data lie. Although there is a clear distinction between the average for trafficked and non-trafficked cells for all of the seven parameters except Sr2, the large error bars demonstrate the high variability in the measurements. The substantial overlap between the trafficked and non-trafficked error bars indicates that without prior information, in most cases, given another measurement it would be impossible to determine whether the measurement had come from a trafficked or non-trafficked cell with any certainty.

It is also interesting to note that for a number of the parameters (Vmc, c2 and Sp) the non-trafficked average seems to show a distinct upwards trend as number of passes increases, whereas the average for the trafficked cells shows no clear upwards or downwards trend. This indicates that the measurements from the 3D camera are detecting changes in the non-trafficked cells as passes increase, but not in the trafficked cells. We can suggest no reason for this pattern.

4.2.3 Can the parameters be used to detect changes in condition?

Section 4.2.2 showed that the statistical analysis was unable to identify any strong absolute relationships between the parameter values and the number of wheelpasses (which was being used as a proxy for wear and surface disintegration). However, it was possible to investigate other potential ways of using the parameters.

Instead of looking at the absolute parameter values, which were seen in Figure 49 to have substantial overlap, the changes between successive parameter values were investigated. These are shown in Figure 50 and Figure 51 below for a selection of the shortlisted parameters (the change values have been squared to remove negative values as the fact that the cell parameter value had changed was of more interest than whether it had increased or decreased at this stage).

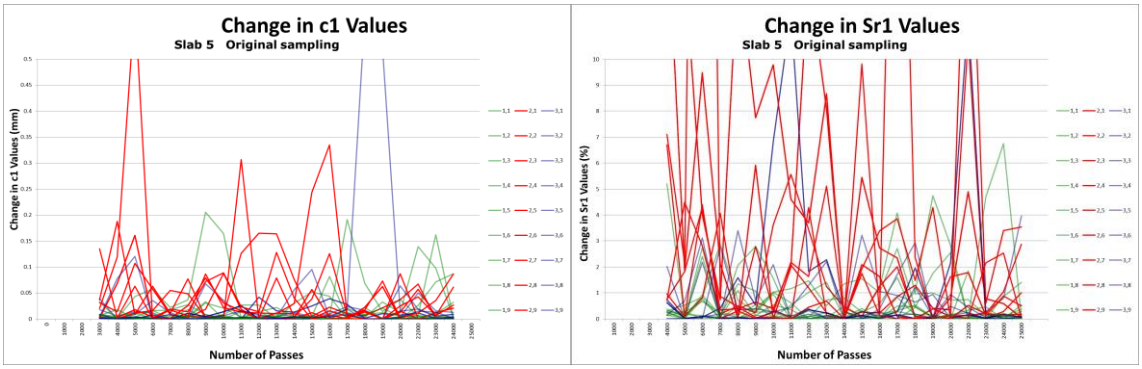

Figure 50: Values of change in parameter c1 and Sr1, compared to parameter value measured 1000 passes before. Red lines show trafficked cells, blue and green lines show values from un-trafficked cells.

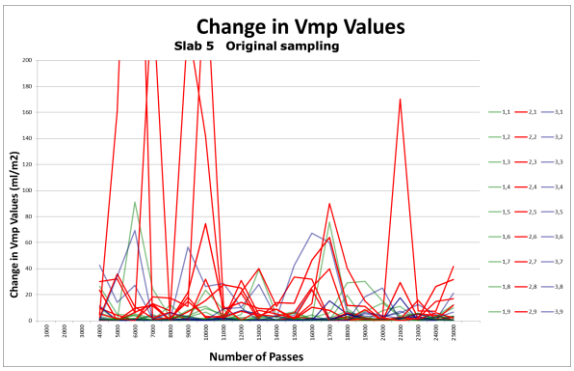

Figure 51: Values of change in parameter Vmp, compared to parameter value measured 1000 passes before. Red lines show trafficked cells, blue and green lines show values from un-trafficked cells.

It can be seen that the values of parameters c1 and Sr1 seem to change much more dramatically on trafficked cells (red) of the samples than on untrafficked cells (blue and green) of the samples. Conversely, Figure 51 shows that the levels of change seen in parameter Vmp were not so well separated according to the levels of trafficking experienced by the cells.

To demonstrate how we might use such parameters to track changes in condition we have examined the use of the parameters shown in Figure 50 to suggest a potential change parameter ΔP. By scaling and combining the measured changes in parameters c1 and Sr1 we define parameter ΔP:

$$\Delta \boldsymbol{P} = \mathbf{1000}(\boldsymbol{dc^2}) \times \mathbf{10}(\boldsymbol{ds^2}) \qquad \textbf{Equation 1}$$

Where $dc = c1_t - c1_{t-1}$,

And $ds = Sr1_t - Sr1_{t-1}$

With $c1_t$ being the value of parameter c1 at time t, and $c1_{t-1}$ being the value of c1 at time t-1, or the previous measurement value. Similarly for parameter $Sr1_t$ and $Sr1_{t-1}$.

This parameter produces higher values on cells which have been trafficked than on untrafficked cells, suggesting that it may be useful in identifying those cells where the surface condition of the sample has changed. Figure 52 shows a display of conditionally formatted values of this parameter in each cell for a number of measurements following trafficking.

Although these have not been shown statistically to relate to the levels of trafficking the samples had obtained, they can potentially be used to distinguish between parts of surfaces which have changed, and parts which have not.

Note: the parameter described here utilises standard parameters extracted using the MountainsMap software. These parameters are well defined and conform to various ISO specifications and as such were relatively simple and straightforward to produce. The change parameter presented here is an example of a possible approach using these standard parameters to demonstrate a) the types of things that can be done with the data, and b) that trafficked cells within the samples do indeed change more than untrafficked cells.

It may be possible to develop bespoke surface disintegration parameters which are specifically tuned to look for signs of missing, or loosening aggregate within the measured data. Such methods may be similar to a 3-D implementation of the Stoneway approach discussed previously, in that instead of looking for general signs that the surface profile within a small area has changed, they may look for more specific signs of aggregate removal, and may give more spatial information regarding the changes taking place. It has not been possible to develop such bespoke parameters in this work.

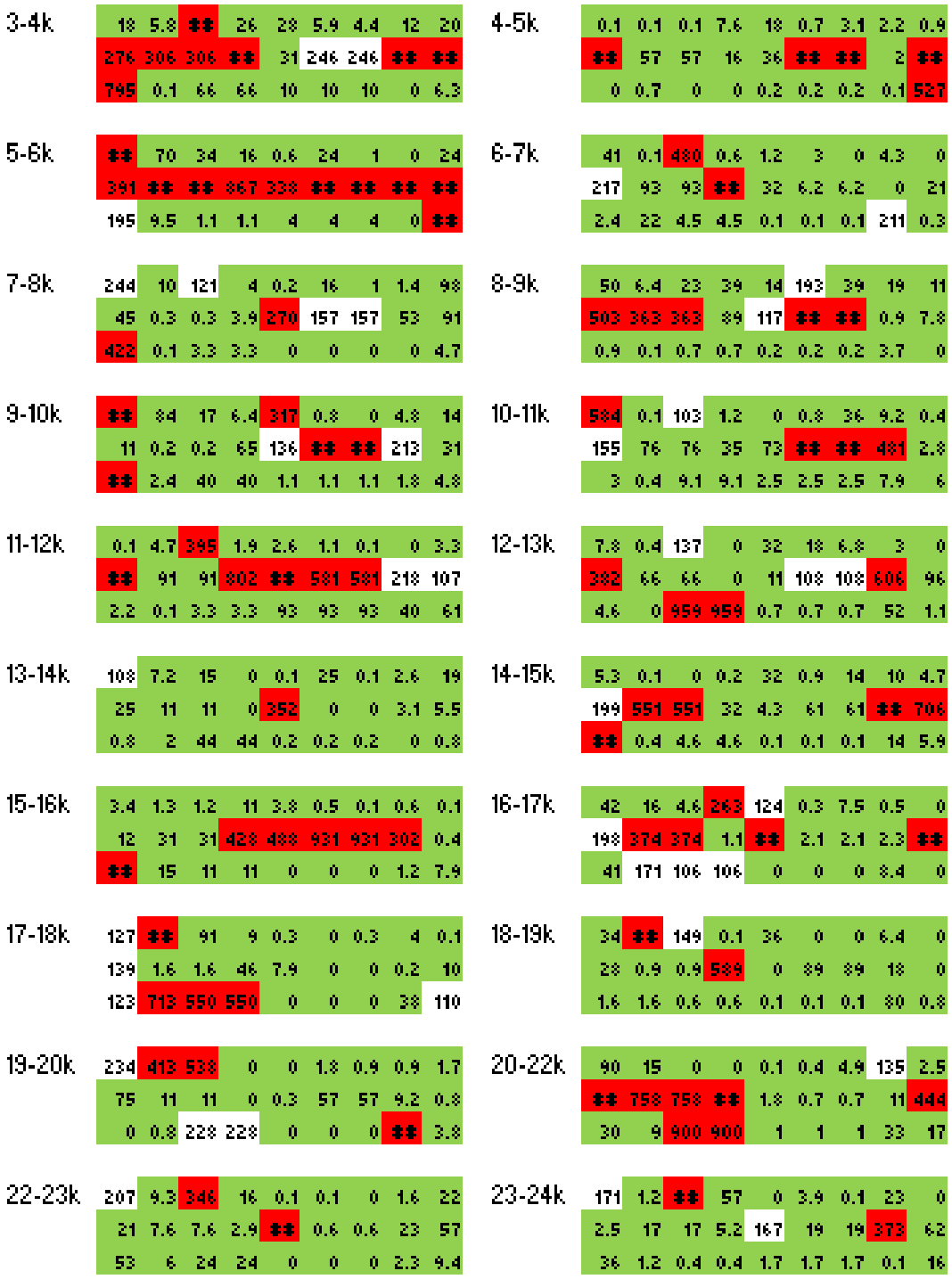

Figure 52: Conditionally formatted display of sample cell ΔP values after different levels of wear. Red shows cells with ΔP>250, green shows cells with ΔP<100.

Cells coloured red have ΔP values greater than 250, while those coloured green have values less than 100. Those with values between 100 and 250 are left uncoloured.

Note that this shows the detected change in sample surface parameters between successive measurements, not a measure of the absolute condition of the sample. Due to the nature of the accelerated wear and testing undertaken it is not expected that the pavement should necessarily change more rapidly as time and testing goes on, and therefore there is no expectation that more red cells should be present in the data

showing change following higher numbers of wheelpasses. For the purposes of this test, each dataset shows data following 1000 more passes from the previous set, and whether or not that had changed – no attempt is made to relate the measured data back to the initial baseline condition following the initial wear of the surface.

It can be seen that the majority of the red cells, with high ΔP values, are located in the middle row, where the sample was subjected to wear. This is particularly noticeable in the data obtained after 6000 passes, where all the middle cells were red. There were only 2 occasions where the untrafficked cells exhibited more cells with high ΔP values than the trafficked cells.

Of the 378 untrafficked cell parameter values (18 cells x 21 measurements of change), only 31 of them (8.2%) were over 250. Of the 189 trafficked cells (9 cells x 21 measurements of change), 61 of them (32.2%) had ΔP values over 250.

Figure 53 shows the cumulative distributions of the trafficked and untrafficked cell change values for different ΔP values. This clearly shows that more of the trafficked cells exhibit high ΔP values than the untrafficked cells. Over 85% of untrafficked cells have ΔP values <100, whilst only 58% of trafficked cells have low ΔP values.

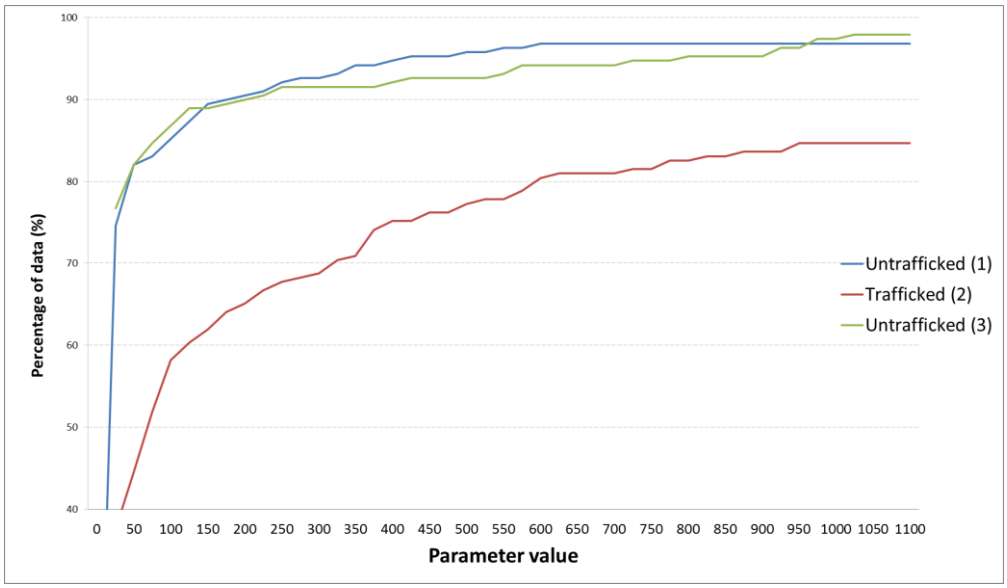

Figure 53: Proportions of sample cells where change parameter is less than parameter values shown along x-axis for each of the 3 rows of cells.

The ΔP parameter is more likely to report a high value on cells that are undergoing wear and actually changing condition than it is on cells which are not changing. On slab6, which was created with a weaker bitumen mix, so was likely to be more susceptible to changes, 75% of the untrafficked cells had ΔP values <100, while 18% had values >250. On the trafficked cells these values were 49% <100, and 42%>250.

This could potentially be very useful in terms of identifying those areas of a pavement or network where the condition of the pavement has changed. Because the parameter is using measurements made at a much finer resolution than are currently available it could be that such a parameter can flag areas which are changing before they reach a state which is detectable using current techniques and tools. This has not yet been demonstrated on network data. However, it is anticipated that the number of locations where surface disintegration is taking place will be much smaller than the number of

locations where it is not taking place, and a 5 - 10% false positive rate will produce a large amount of hits on parts of the network which are not deteriorating.

4.2.3.1 Effect of data resolution on change parameter

The measurements made by the Breuckmann SmartSCAN camera were made at sub-mm resolution (4.1.3). It is known that data at this level of resolution would be very difficult or impossible to supply from a traffic speed survey using currently available technologies. By resampling the data prior to the extraction of the parameters it has been possible to simulate the data which would be collected using systems with different data collection capabilities. The data has been resampled to produce output parameters based on measurements made at 1mm, 2mm, 5mm and 10mm measurement point spacings.

Table 6 shows the threshold levels chosen for categorising the low and high values of the ΔP parameter, and the proportions of the trafficked and untrafficked cells in each category. The threshold levels have been selected to try to produce similar levels of trafficked cells in the high and low categories at all resolutions. Changing the thresholds in this way also affects the proportions of the untrafficked cells on each category. The thresholds were also chosen in order to maintain a large distinction between the trafficked and un-trafficked data proportions classed as high or low. Additionally, the thresholds were chosen to be 'round numbers' as it was felt that tuning the thresholds to provide greater control over the proportions of the data in each category would perhaps give a false impression of the significance of the results. The threshold values chosen in this research are not necessarily suitable for use on network data, but are merely a useful and simple method for demonstrating that the distribution of change parameter values is different on trafficked and un-trafficked cells within the samples tested, and that the distinction between the trafficked and untrafficked cells drops as the data resolution becomes more coarse.

Table 6: Effect of data resolution on performance of change parameter

Data resolution	ΔP Thresholds	Untrafficked cells	Trafficked cells
Original	**<100**	86.0%	58.2%
	>250	8.2%	32.3%
1mm	**<100**	91.0%	64.6%
	>250	5.0%	25.9%
2mm	**<150**	88.6%	57.7%
	>250	6.9%	36.5%
5mm	**<200**	60.8%	35.4%
	>3000	11.6%	24.3%
10mm	**<1000**	55.3%	45.0%
	>7500	19.6%	30.7%

These figures are displayed graphically in Figure 54 and Figure 55, below. It can be seen that although there are still clear differences between the proportions of high values

found on the trafficked and untrafficked cells, the distinction between the trafficked and untrafficked cells falls as the data resolution is lowered below 2mm.

As was noted before, the proportion of the network which is likely to be deteriorating is small compared to the proportion where the condition will be stable. If the parameter as calculated on deteriorating cells is not sufficiently distinct from the values calculated on stable cells then there will be a huge number of false positives reported, undermining the usefulness of the parameter.

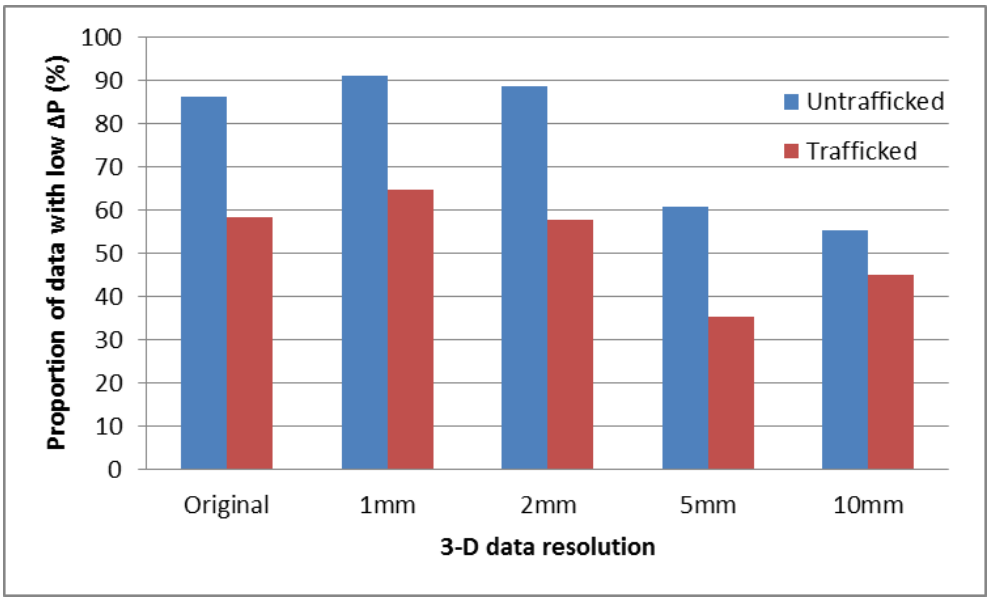

Figure 54: Percentages of untrafficked (blue) and trafficked (red) cells with ΔP values below low threshold.

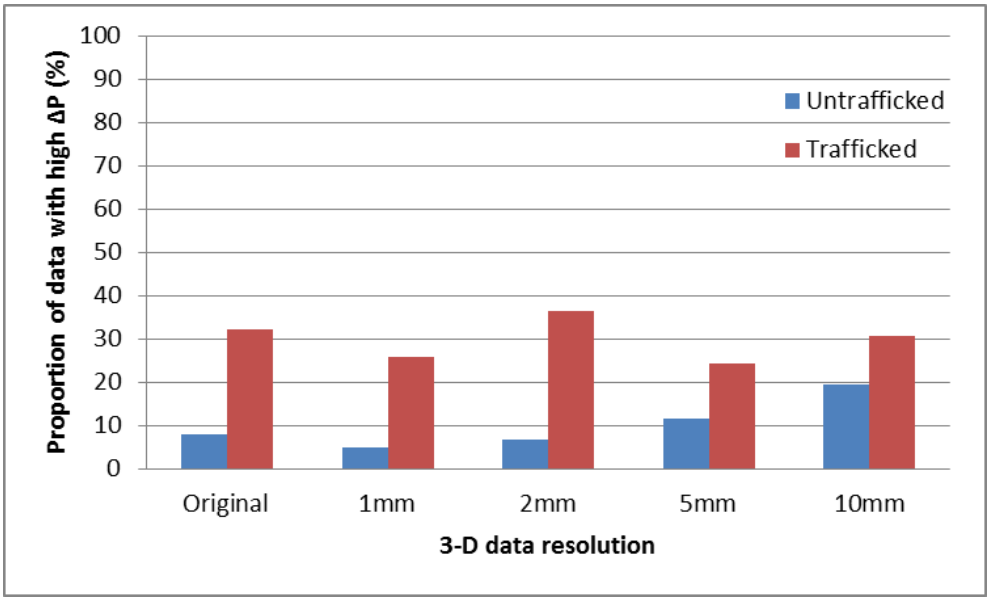

Figure 55: Percentages of untrafficked (blue) and trafficked (red) cells with ΔP values above high threshold.

For the ΔP parameter to be useful as a way of discriminating between those parts of the pavement which have changed, and those which have not, it appears that the input data would need to be supplied at a resolution no worse than every 2mm, longitudinally and transversally. With data at a lower resolution than this the likelihood of a high value coming from an untrafficked, as opposed to a trafficked cell is 50 - 66%.

5 Summary, Conclusions and Recommendations

This research has investigated the potential to develop methods to detect surface disintegration (fretting) in its early stages. A literature review has confirmed that, although there is research taking place elsewhere to improve the ability to detect this defect, current approaches are focussed on the identification of the defect when well developed and hence clearly present. There have not been any significant leaps forward from the development of algorithms used in TRACS to identify the defect at the network level.

In this work we have approached the development of methods to detect surface disintegration in its early stages from the viewpoint of measuring changes in the surface of the road at a high level of detail. It has been assumed that the identification of small changes associated with loss of stone could be used to highlight lengths where the onset of more significant deterioration is imminent.

Therefore we have considered two requirements: the need to be able to align and compare data collected from separate surveys to a high level of accuracy; and the need to be able to measure the surface of the pavement at a level of detail where it would be possible to identify the loss of stones.

5.1 Alignment of data

For the alignment of data we commenced with the application of GPS combined with longitudinal profile to align survey data along the length of the survey, and then added the use of transverse profile to improve the automated alignment of data across the surveyed lane, hence compensating for the effects of driving line. This has produced datasets which are very well aligned. Although initial testing found problems with noise in the transverse alignment we have alleviated this problem to some extent by applying logical rules to the transverse alignment derived from physical limitations on the amount and rate that a survey vehicle can moved across the surveyed lane.

We have focussed on the application of alignment to the detection of surface disintegration in its early stages. However, the use of high accuracy alignment could have significant potential in the general assessment and prediction of condition, as it could be used to determine whether any pavement has changed or deteriorated between surveys. However, the alignment work successfully undertaken herein has only been demonstrated and tested at the laboratory (test track) level, and has not yet been linked to the measurement of change. It is therefore recommended that the successful developments of this work be taken forward to larger scale testing on the network. This larger testing would refine the alignment process (both transversely and longitudinally) and overcome the technical challenges associated with data collected in real-world (not laboratory) conditions. However, even if the remaining technical challenges to alignment are overcome there is also a need to consider how the method could be applied in practice. High-accuracy alignment requires the availability of raw survey data with which to undertake the transverse and longitudinal alignment. This large volume raw data is not routinely available or handled by the HA. Therefore further work would be required to investigate and develop the data handling and processing methods required to implement the technique at the network level.

5.2 Use of high resolution profile

The investigation into the use of high resolution profile to detect the early stages of surface disintegration has had to address two challenges: how to develop an objective method of introducing and developing surface disintegration on real pavement samples; and how to identify a measure of pavement shape that can be used to quantify this deterioration.

The laboratory testing undertaken to address the first challenge found that there is no standardised way to artificially produce surface disintegration in a lab which correctly and efficiently replicates the wear which occurs on real pavements. Our solution, using the MLPC rutting machine, did introduce surface disintegration, but also created other deterioration (rutting) which has complicated the shape analysis. Although this was not an original objective of this research, our work highlights the need for further research into a robust method to test pavement surfaces in the development of surface disintegration. It is understood that the CEDR research programme for 2015 is intending to commission research in this specific area.

The research into the use of profile (shape) to detect surface disintegration has shown that the SmartSCAN system is able to measure at a sufficient level of detail to (visually) observe deterioration in the shape data. We have investigated the use of a large number of standard surface shape parameters to determine if any of these could be used to quantify surface disintegration at any stage, or the change in surface disintegration with trafficking. The statistical analysis has shown that the mean values of the surface shape parameters on trafficked and un-trafficked samples are clearly different, but the variability in individual measurements prevents them from being used to quantify deterioration at any specific stage of trafficking. However, examination of the change in the surface shape parameters as trafficking increases has been more successful. By combining and scaling surface shape parameters we have demonstrated that it should be possible to detect change resulting from surface disintegration. However, the research has not demonstrated a robust way of doing this, as there is quite a large degree of uncertainty in the reported results. This may be because the individual surface shape parameters employed in the change measurement are not themselves sensitive enough to the way that the shape of the pavement changes when stones are lost (which has been made more difficult to investigate as a result of the combination of rutting and surface shape introduced by the MLPC rutting machine). Therefore, although this work has not been completely successful in delivering a shape measure, the work has demonstrated that there is a strong potential for the use of change in shape to detect the progression of surface disintegration. There would therefore be benefit in further development of the shape parameters to fine-tune them for the specific changes in shape that result when stone loss occurs. These more sensitive parameters would then help to improve the robustness of the change measure proposed in this work.

Acknowledgements

The authors would like to thank the following for their help and advice throughout this research:

- Alex Wright, for technical advice and oversight throughout the project, and for review of the final report;
- Colin Jones, Cliff Nicholls and Paul Sanders for advice about pavements and deterioration;
- Jean Iaquinta and Alan Dunford for advice and feedback on the experimental design
- Neal Harwood, John Prime and Karl Morosiuk for assistance with the laboratory work, data collection and processing;
- Lena Weaver, Dean Wright and Nathan Dhillon for assistance with collecting and processing HARRIS2 data for development and testing of data alignment techniques.
- Louise Lloyd for statistical advice.

References

Ahmed, M. F., & Haas, C. (2010). The potential of low cost close range photogrammetry towards unified automatic pavement distress surveying. *Proceedings of The 89th Annual Meeting Of The Transportation Research Board (DVD)*, (pp. 11-15). Washington D.C.

Bitelli, G., Simone, A., Girardi, F., & Lantieri, C. (2012). Laser scanning on road pavements: a new approach for characterizing surface texture. *Sensors* , 9110-9128.

Elunai, R., Chandran, V., & Mabukwa, P. (2010). Digital image processing techniques for pavement macro-texture analysis. *Proceedings of the 24th ARRB Conference: Building on 50 years of road transport research* (pp. 1-5). Melbourne: ARRB Group Ltd.

Furness, G., & Wright, A. (2007). *The automatic assessment of erosion of high friction surfaces, UPR IE/045/07.* Crowthorne, UK: TRL ltd.

Huurman, M., Mo, L. T., & Woldekidan, M. F. (2010). Porous Asphalt Ravelling in Cold Weather Conditions. *International Journal of Pavement Research & Technology, 3*(3).

Jiang, X., Scott, P., Whitehouse, D., & Blunt, L. (2007, July 5). Paradigm shifts in surface metrology. Part 1. Historical philosophy. *Proceedings of the Royal Society A: Mathematical, Physical and Engineering Science, 463*(2085), 2049-2070.

Laurent, J., Hebert, J. F., Lefebvre, D., & Savard, Y. (2012). Using 3D laser profiling sensors for the automated measurement of road surface conditions (ruts, macro-texture, raveling, cracks). *7th Rilem International Conference on Cracking Pavements.* Delft, The Netherlands: RILEM.

Mathavan, S., Rahman, M. M., Stonecliffe-Jones, M., & Kamal, K. (2014). Pavement raveling detection and measurement from synchronised intensity and range

images. *TRB 2014 Annual Meeting.* Washington D.C.: Transportation Research Board.

Mays, C., Wright, A., & Furness, G. (2006). *Road surface texture inspection using high resolution transverse profile measurements, UPR/IE/100/06.* Crowthorne, UK: TRL Ltd.

McRobbie, S., Iaquinta, J., & Wright, A. (2009). *identification and assessment of fretting on different types of pavement surfaces using multiple line texture measurements.* Crowthorne, UK: TRL Ltd.

McRobbie, S., Iaquinta, J., & Wright, A. (2011, December). *Assessment of pavement Surface Disintegration at Traffic Speed - Phase 1 status report.* Crowthorne: TRL Ltd.

McRobbie, S., Iaquinta, J., Kennedy, J., & Wright, A. (2013). *Detection of changes in pavement texture condition using high resolution 3D surface measurements.* Wokingham: TRL Limited.

McRobbie, S., Wright, A., Iaquinta, J., Scott, P., Christie, C., & James, D. (2010). Developing New methods for the Automatic Measurement of Raveling at Traffic-Speed. *11th International Conference on Asphalt Pavements (ISAP).* Nagoya, Japan.

Scott, P., Radband, K., Zohrabi, M., Sanders, P., McRobbie, S., & Wright, A. (2008). Measuring surface disintegration (ravelling or fretting) using traffic speed condition surveys. *7th International Conference on Managing Pavement Assets.* Calgary: TRB.

van Ooijen, W., van den Bol, M., & Bouman, F. (2004). High-speed measurement of ravelling on porous asphalt. *5th Symposium on Pavement Surface Characteristics - Roads and Airports (SURF).* Toronto, Canada.

Wang, K. C., Gong, W., Tracy, T., & Nguyen, V. (2011). *Automated Survey of Pavement Distress Based on 2D and 3D Laser Images.* Arkansas: No. MBTC DOT 3023.

Wang, W., Yan, X., Huang, H., Chu, X., & Abdel-Aty, M. (2011). Design and verification of a laser based device for pavement macrotexture measurement. *Transportation Research Part C*, 682-694.

Wright, A. (2004). *The use of surface texture measurements to identify fretting on Hot Rolled Asphalt, PR/INN/41/04.* Crowthorne, UK: TRL Ltd.